Safety evaluation of lashed trailer motions in ferry operations under rough sea conditions

Sasa, Kenji
Lee, Sangwon
Shimada, Ryotaro
Takagaki, Toru
Terada, Daisuke

(Citation)
Ocean Engineering,275:114114

(Issue Date)
2023-03-10

(Resource Type)
journal article

(Version)
Accepted Manuscript

Safety Evaluation of Lashed Trailer Motions in Ferry Operations under Rough Sea Conditions

Kenji SASA[1], Sang-Won LEE[1*], Ryotaro SHIMADA[2], Toru TAKAGAKI[3], and Daisuke TERADA[4]

1 Graduate School of Maritime Sciences, Kobe University, Kobe, JAPAN
2 Penta-Ocean Construction, Co., Ltd., Tokyo, JAPAN
3 Nomura Research Institute, Ltd., Tokyo, JAPAN
4 National Defense Academy, Yokosuka, JAPAN
* Corresponding Author, e-mail: leesw@port.kobe-u.ac.jp

Abstract

Safety evaluation of a lashed trailer on the cargo deck of ships is essential for ferry operations. Although ferry accidents have occurred worldwide, few studies have focused on the dynamic analysis of trailer motion in irregular sea states. To date, effective counterapproaches have not been established. Thus, first, ferry masters were interviewed to summarize the difficulty in cargo management during rough sea voyages. Second, a modified simulation model of lashed trailer motions was constructed to evaluate the safety of cargo management, considering wave, seakeeping, and trailer motion simulations. Few studies apply the model to the irregular sea state in actual seas, using a combination of three different kinds of models. A simulation was conducted to analyze the collapse of a trailer loaded on a ferry in high waves owing to rapidly developing atmospheric pressures. Essentially, the model can reproduce the collapse of trailers, especially when a shift in the center of gravity is considered when accelerations occur in loaded cargo inside trailers. The model enables the estimation of trailer motions and lashing wire tensions in ferry operations, considering suitable lashing arrangements.

1. Introduction

Ferries or roll-on/roll-off (Ro-Ro) ships have undoubtedly contributed to the development of efficient and environment-friendly transportation worldwide for decades, as they enable consistent transportation at sea and on land, similar to short-distance container transportation. Some routes are located inland, while others face open seas. Naturally, ships are influenced by wind waves that affect the motion of the ship, speed loss, and other parameters. Optimal ship routing is applied to short-distance ferries to avoid rough weather conditions, such as atmospheric depressions (Takashima et al., 2009; Grifoll et al., 2016 and 2018). Some studies have been conducted on passenger ships to reduce roll motion from the viewpoint of comfort against seasickness by using fin stabilizers or anti-rolling tanks, amongst other devices (Perez and Goodwin, 2008; Liang et al., 2022). However, they do not necessarily provide completely safe and efficient voyages. Operators of domestic shipping services, including ferries, monitor the forecasted wave and wind values. If rough sea conditions are forecasted and the voyage time is within a day, the shipping services are usually canceled. Thus, accidents can be avoided if the weather forecast is reliable. However, forecasting technology still faces difficulty with some patterns of low pressures that develop rapidly. Each shipping company sets a limit to conditions, such as forecasted wave height or wind speed, for safe sailing. Nevertheless, weather uncertainty still makes the decision difficult in an actual operation.

Ferries and Ro-Ro ships also require efficient cargo management. Trailers are mainly loaded on cargo decks inside ships and are usually lashed with several wire ropes. Since the securing of trailers is relatively unstable owing to their structure, the trailers move when the ships face rough seas. Methods for estimating the wire tension, such as the static method (Zhang et al., 2019), which calculates wire tensions by solving the balance of mooring forces without considering the dynamic behavior of trailers, have been proposed. The Japanese Ministry of Land, Infrastructure, Transport, and Tourism (2011) has issued guidelines for securing cargo in ferries or Ro-Ro ships as a summary of the stranded Ferry Ariake accident in Japan. The summary describes 10 other accidents of ferries, which occurred between 2004 and 2009 with large heel angles of more than 25°, and the static analysis of lashing forces and moments in detail. However, the authors believe that these static analyses are not sufficient to evaluate the actual behavior of lashed trailers owing to ship motion in actual seas. Some studies have focused on dynamic analysis methods for lashed trailers under given ship motion conditions (Turnbull and Dawson, 1994, 1997, and 1999; Turnbull, 2000; Poulios et al., 2008 and 2009). Numerical theories were provided as a time-domain analysis of equations governing the trailer motions. However, the time series of wire tension was computed only for 30–60 s for regular roll and pitch motions. No studies have simulated the motion of trailers in actual seas with irregular waves. Instead, erroneous descriptions in formulas found during the validation process were confirmed by the authors. Thus, the errors have been corrected through comparison with previous studies, and a safety evaluation against lashed trailers on the cargo deck inside the ship was conducted in this study.

Section 2 discusses the cargo management situation investigated by interviewing Japanese ferry companies, especially those conducting rough sea voyages, and difficulty in cargo management was observed to be strongly related to the accuracy of weather forecasts. In Section 3, numerical simulations of the lashed trailer motions are reconstructed, including corrections to some formulas. The motions of the ferries are estimated by the seakeeping model, enhanced unified theory (EUT) (Kashiwagi, 1992 and 1997), and third-generation wave model WaveWATCH III (WW3) (Tolman, 1989 and 2014). In Section 4, the cargo collapse accident of 2009, on a large ferry along the

Pacific Ocean in Japan, is reproduced using the numerical model presented in Section 3. In Section 5, a collapse of the lashed cargo is considered by analyzing the simulated results. Furthermore, the possibility of cargo shifting inside the trailer is also considered by applying the experimental results of cargo collapse for piled cardboard boxes (Saito et al., 1996, 1997 and 2002). Section 6 summarizes the safety evaluation of lashed cargo in ferries or Ro-Ro ships as the conclusion to this study.

2. Cargo management for ferry transportation

Sasa et al. (2005) studied the difficulties faced by the Japanese ferry line while entering and departing harbors when swells or low atmospheric pressure approach. Simultaneously, it was observed that a ferry operator experiences difficulty in cargo management, especially when the air pressure decreases below 1,000 hPa. Thus, two ship masters of a Japanese ferry company were interviewed in this study to investigate the situation. The company operates four ferries between O Port (Ibaragi Prefecture) and T Port (Hokkaido Prefecture), and the ship route lies in the Pacific Ocean of Northern Japan, as shown in Figure 1.

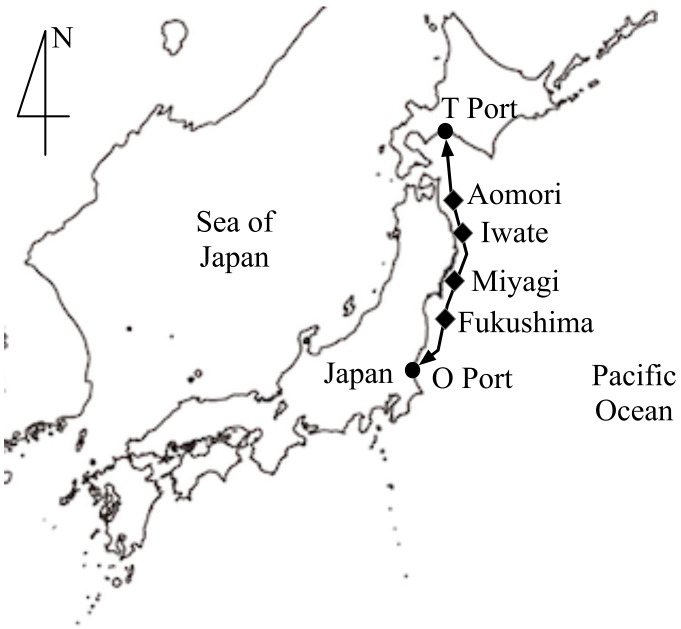

Figure 1 Voyage route of ferries run by the ferry company

The main points of cargo management and ship operations are summarized as follows.

(1) Since cargo decks are divided into lower and upper decks, cargos on the upper deck sustain more serious damage.

(2) Cargos placed on the fore and aft sections also sustain large damages, with most frequent damage in those placed on the aft. Ship roll motion mainly influences the safety of the lashed trailer. Additionally, ship pitch motion was assumed to be the alternative factor causing the damage at the fore and aft. Therefore, the coupling of these rotational ship motions leads to larger trailer motions in aft section of the ship.

(3) However, cargos are not loaded in certain spaces of the fore and aft sections when rough weather is forecasted.

(4) One of the operating ferries, named Ferry D, experienced a very serious accident in April 2009. Ferry D

encountered a rough sea and nearly 100 trailers collapsed. The main factor was reported to be the insufficient management of metacenter height. However, the factor did not justify the reason why the trailer motion cannot avoid accidents just by arranging the metacenter height.

(5) Accidents occur at a significant wave height of 5 m, while the maximum wave height is approximately 10 m, twice the wave height causing accidents. Furthermore, an extreme wave height, larger than that in 1,000 waves, can occur. Thus, the irregularity of waves may cause accidents.

(6) Furthermore, wave period and direction of waves are important. Remarkable ship motions are observed when the wave period is greater than 10 s.

(7) Low air pressure periodically moves eastward from continental China during the winter season, a typical winter weather pattern defined as Pattern 1 in Figure 2. Thus, waves do not mature in the Pacific Ocean and the ship motions are not very large. Conversely, the wave period tends to be longer when low air pressures move northeasterly at a slow speed (Sasa et al., 2014), defined as Pattern 2 in Figure 2. Therefore, ships must pay attention to such weather condition. The results are shown in Figure 2.

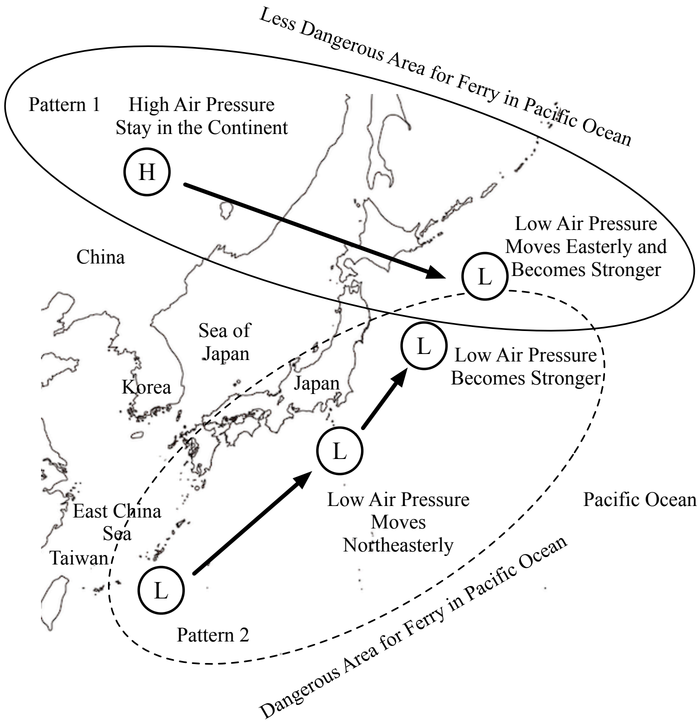

Figure 2 Weather patterns around Japan during winter

(8) Since speed loss occurs in rough seas, the ability of the fin stabilizer reduces simultaneously when the ship speed reduces to less than 18 knots, where voyage speed is set at 25 knots. Thus, roll motion cannot be reduced in rough seas because if the engine power is increased to prevent speed loss, pitch motion will be dangerously high. A trade-off relationship exists between the roll and pitch motions causing difficulty in ship operation.

(9) The safety of a voyage must be judged 24–48 h before departure, for which ferry companies use multiple weather-forecasting services. However, the amount of available information is insufficient, which often leads to empirical decisions. Real-time wave information along the voyage routes is available from the Nationwide Ocean Wave

information network for Ports and HAbourS, NOWPHAS (Kawai et al., 2020). The information is more useful if the maximum wave height is known from the irregular wave history of 1,000 waves.

(10) A shallow water area exists outside O Port where the wave height appears to be large. The fairway is narrow and requires turning around a long breakwater. Maneuvering difficulty can occur for ships having a large heel angle of approximately 25°, which influences the lashed trailers in addition to offshore voyages.

(11) Vehicle cargos are commonly loaded in ferries and Ro-Ro ships. However, the positions of the main engines differ between ships. Thus, the properties of the ship motions are slightly different.

The importance of wave forecasting has been emphasized in the summary, and the real-time wave information system, NOWPHAS, contributes to operational decisions. The information received from the system has been given significant values. The maximum value was obtained for a time length of 20 min. For an assumed wave period of 5–15 s, the number of waves was 80–300. However, ship masters believe in evaluating the maximum wave height over a longer period, such as 1,000 waves for 5,000–15,000 s. Thus confirming that safety should be validated in irregular sea states during voyages.

3. Numerical simulations of lashed trailers on the cargo deck of a ferry in an actual sea

In this section, theoretical descriptions are presented for the safety evaluation of lashed trailers in ferries and Ro-Ro ships in actual seas. The lashed trailer motions are generated when ship motions occur. Thus, the lashed trailer motions can be estimated if the ship motions are estimated by applying estimated wave spectrum and frequency response functions.

The mathematical model in this study is constructed in 5 steps, as shown in Figure 3. First, the directional wave spectrum is estimated to represent the actual sea states. Then, the ship motions are estimated as the product of the directional wave spectrum and the squared frequency response functions, which are simulated by the EUT model. Next, the centrifugal and tangential forces are calculated at the positions of each trailer owing to the ship motions, which could cause the trailer motions. The trailer motions affect the suspension and wire rope connected to the trailer, generating a suspension force and rope tension. Finally, the equations of motion are solved for the total force acting on the lashed trailer.

The main coordinate systems used for the ship and trailer motions are presented in Figure 4. The directional wave spectrum is estimated using the earth-fixed-axes in Step 1. The origin of the ship hull-fixed axes is located at the ship center of gravity, which is used for the ship motions and centrifugal and tangential forces in Steps 2 and 3. The trailer motions are solved in the trailer-fixed axes for the forces on the suspension and wire rope in Steps 4 and 5.

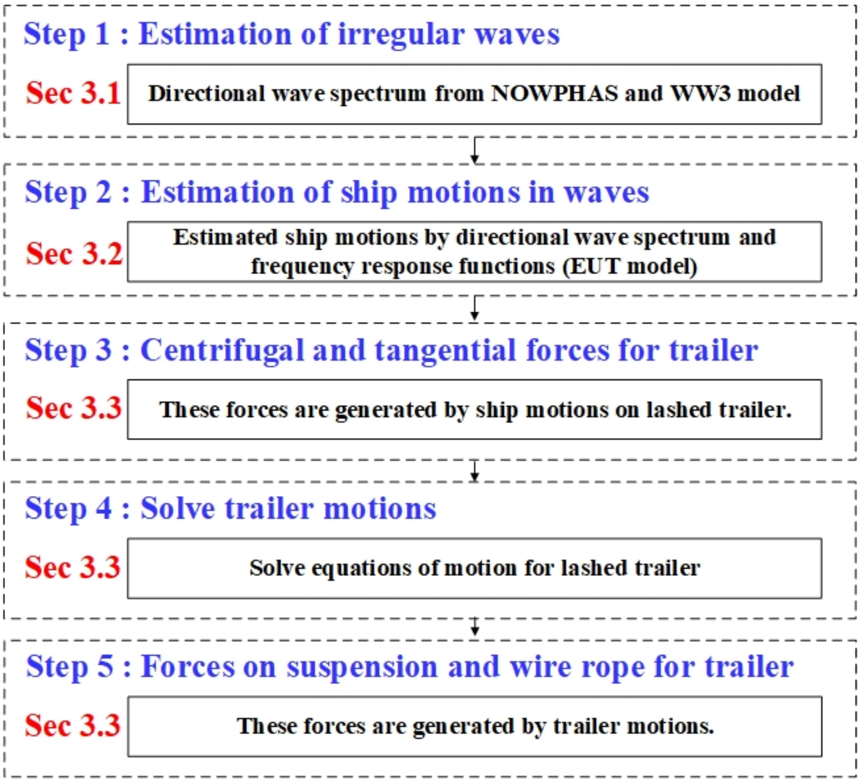

Figure 3 Flowchart of mathematical model for presented method

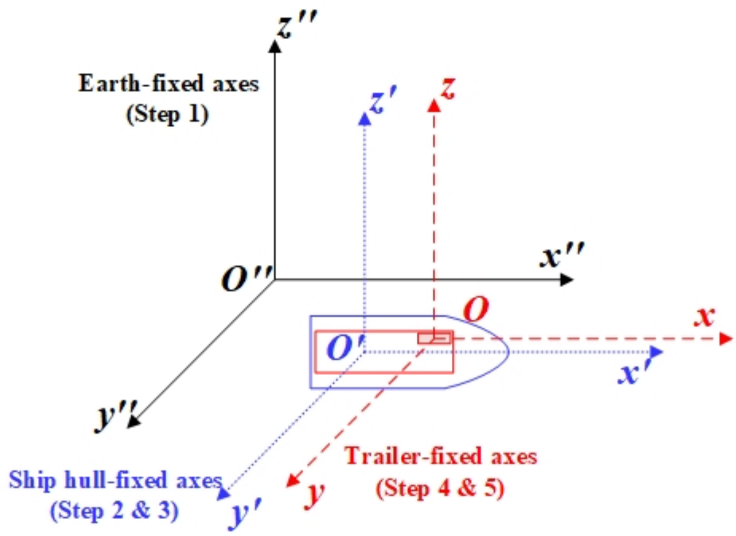

Figure 4 Coordinate systems used in ship and trailer motions

3.1 Estimation of directional wave spectrum

To estimate the motion of a lashed trailer in an actual sea, it is necessary to reproduce ship motions under an irregular sea state. Since an actual wave forms a directional spectrum propagating in various directions, a directional wave spectrum is required for the estimation of ship motions. Thus, in this study, two types of directional wave spectra were estimated and compared. The first was the spectrum numerically simulated by the WW3 as an output of the reanalysis wind data, while the other was the wave directional spectrum estimated using the measured surface elevations in the NOWPHAS system combined with the cosine-squared directional function.

(1) WW3

As aforementioned, the WW3 is a third-generation phase-averaged wave model for wave hindcasting simulations (Booij and Holthuijsen, 1987; Tolman, 1989 and 2014), with wind input as the most dominant factor. Chen et al. (2020) compared the simulated results of waves in rough sea voyages of a bulk carrier between the National Centers for Environmental Prediction Final (NCEP-FNL) (Kalnay et al., 1996) and the European Center for Medium-Range Weather Forecast (ECMWF) reanalysis database (Dee et al., 2011). Furthermore, Lee et al. (2022) showed that anchored ship motions can be reproduced more accurately with NCEP-FNL than with the ECMWF reanalysis. Thus, NCEP-FNL was used as the wind input for the WW3 simulation in this study. Ship motions can be estimated as the product of wave directional spectra and frequency response functions in each wave direction. Thus, the directional interval was defined as 10° for covering all directions. The range of wave frequencies was set at 0.05–0.28 Hz for every 0.01 Hz. To initiate the simulation of the WW3, a spin-up simulation must be conducted a month in advance to the start time. The wave directional spectrum was obtained by solving the governing equation of the WW3 for a defined computing region. The distributions of the significant wave height and main wave direction have been summarized from the computed results of the directional wave spectrum. The WW3 model was numerically solved for the directional wave spectrum of each frequency and direction, $E_W(f,\theta)$.

(2) NOWPHAS

The directional wave spectrum is a wave information based on the measured surface elevation in the offshore global positioning system (GPS) buoy of the NOWPHAS system. The measured surface elevation in each time step was transformed into a frequency spectrum by fast Fourier transformation. However, no information on directional dispersion was included in the NOWPHAS system other than the main wave direction. Thus, the frequency spectrum was converted to a wave directional spectrum by multiplying it with the theoretical directional function as (Hughes, 1985)

$$E_W(f,\theta) = S_W(f)D(\theta), \tag{1}$$

where $E_W(f,\theta)$ is the directional wave spectrum, $S_W(f)$ is the wave frequency spectrum, $D(\theta)$ is a directional function, f is the frequency, and θ is the wave direction. $D(\theta)$ satisfies the relationship

$$\int_0^\infty \int_{-\pi}^{\pi} S(f)\, D(\theta) d\theta df = \int_0^\infty S(f) df, \tag{2}$$

$$\text{and } \int_{-\pi}^{\pi} D(\theta) d\theta = 1. \tag{3}$$

From the different types of directional functions, the cosine-squared function was used in this study. The function is defined as

$$D(\theta) = \begin{cases} \frac{2}{\pi} cos^2(\theta - \theta_0), \ for \ |\theta - \theta_0| < \frac{\pi}{2} \\ 0, \ otherwise \end{cases}, \tag{4}$$

where θ_0 is the main wave direction given in the NOWPHAS. The values of $E_W(f, \theta)$ in the WW3 simulation were directly determined as the numerical solution of the governing equations. Conversely, it was necessary to assume a theoretical $D(\theta)$, although $S(f)$ was accurate for the measured surface elevation in the NOWPHAS system. The measured surface elevations were not available when the wave height exceeded a certain value. For this study, the ship motions were estimated from both the wave directional spectra for comparison.

3.2 Estimation of ship motions by directional wave spectrum and frequency response functions

Existing seakeeping models can be used to estimate ship motions that are practically accurate in actual seas, including rough sea conditions (Sasa et al., 2012 and 2017). The frequency response functions of ships are computed by the EUT (Kashiwagi, 1997) for each frequency, wave direction, and ship speed value. The EUT is based on the unified theory (Newman, 1979), which introduces three-dimensional corrections to the two-dimensional strip theory solution. The damping of the ship roll motion is obtained by adding the viscous damping force to the hydrodynamic damping force (Ikeda et al., 1993). This is a practically accurate model for ship motions in actual seas (Kashiwagi et al., 2004) and has also shown good agreement with measured ship motions (Lu et al., 2017; Chen et al., 2020; Sasa et al., 2021; Waskito et al., 2022). Although simulated results are shown in Section 4, measured ship motions were unavailable for rough sea voyages in 2009. Thus, ship motions of the ferry cannot be validated here. Alternatively, the accuracy is discussed for eight cases of measured and simulated ship motions including the EUT for 28,000-DWT bulk carrier in actual seas (Waskito et al. 2022). Significant amplitudes of roll and pitch motions are compared in detail, and the EUT can reproduce them with practical accuracy in various wave conditions and sea areas, except some points. Therefore, the EUT was used to compute the frequency response functions and the ship motions are estimated using Eqs. (5)–(10) as follows.

The directional spectra of ship motions were estimated as the product of the directional wave spectrum and frequency response functions in each wave direction and frequency, as shown in Eqs. (5) and (6), respectively, while the significant amplitudes of the ship motions are given by Eqs. (7) and (8), respectively.

$$E_R(f, \theta) = |R(f, \theta)|^2 E_W(f, \theta) \quad , \tag{5}$$

$$E_P(f, \theta) = |P(f, \theta)|^2 E_W(f, \theta) \quad , \tag{6}$$

$$R_{1/3} = 4.0\sqrt{\int_0^\infty E_R(f, \theta) d\theta df} \quad , \tag{7}$$

$$P_{1/3} = 4.0\sqrt{\int_0^\infty E_P(f, \theta) d\theta df} \quad , \tag{8}$$

where $E_R(f, \theta)$ and $E_P(f, \theta)$ are the directional spectrum in ship roll and pitch motions, $R(f, \theta)$ and $P(f, \theta)$ are the frequency response functions in the wave direction of θ, and $R_{1/3}$ and $P_{1/3}$ are the significant amplitudes in ship roll and pitch motions, respectively. To dynamically analyze the lashed trailer motions, time series of roll and pitch ship motions are necessary and are expressed in Eqs. (9) and (10), respectively.

$$R_{SHIP}(t) = \sqrt{2\sum_{i=1}^{N}\sum_{j=1}^{M} E_R(f_i, \theta_j) d\theta df} \cos(2\pi f_i t - \varepsilon_{Ri} - \varepsilon_i) \quad , \tag{9}$$

$$P_{SHIP}(t) = \sqrt{2\sum_{i=1}^{N}\sum_{j=1}^{M} E_P(f_i, \theta_j) d\theta df} \cos(2\pi f_i t - \varepsilon_{Pi} - \varepsilon_i) \quad , \tag{10}$$

where $R_{SHIP}(t)$ and $P_{SHIP}(t)$ are the time series of the roll and pitch motions of the ship, ε_R and ε_P are the phases in the roll and pitch motions, and ε is the phase of the incident wave. Ship motions in actual seas are focused in this study. This means that ship motions occur in irregular seas, which are simulated by the WW3 model as the directional wave spectrum in frequency domain. Moreover, the EUT computes the frequency response functions in the frequency domain. Ship motions are evaluated as the significant amplitude as defined in Eqs. (7) and (8). Time series of ship motions are necessary to analyze the lashed trailer motions. These are numerically estimated with Eqs. (9) and (10) by generating the random number for the phase of incident wave. Computed time series of ship roll and pitch motions are shown later.

3.3 Equation of motion for lashed trailers on a cargo deck

Although some examples of static analysis of lash trailers have been reported (Ministry of Land, Infrastructure, Transport and Tourism, 2011), the dynamic effects could not be reproduced. Several studies have focused on the dynamic motion analysis of lashed trailers on deck (Turnbull and Dawson, 1994, 1997 and 1999; Turnbull, 2000; Poulios et al., 2008 and 2009). However, these analyses have not been applied to practical ferry operation in actual seas. First, previous studies focused only on ship motions in regular sea states for a 1–2 min length of time, although wave irregularity made the phenomenon strongly dynamic. On the other hand, to consider the irregularity of waves, the time length should be evaluated for longer periods, such as 1,000 waves for 5,000–15,000 s. Second, some of the formulas were modified because the authors found that they were theoretically incorrect in the former studies. The modified models were required for the application to the voyage of a domestic ferry, for approximately 18 h. Occasionally, time series analysis do not converge if the time step of numerical integration is a constant value. Very few studies have been conducted on convergence compared with the numerical integration method using a fluctuating time step. Thus, convergence was also investigated in detail.

The simulation model of the lashed trailer motions was based on Poulios et al. (2008 and 2009) and the detailed descriptions are referenced therein. Figure 5 shows the lashing arrangement for the trailer as defined in this study. The arrangement is defined as symmetrical in both the longitudinal and lateral directions with eight wire ropes. The five modes of lashed trailer motions were analyzed, except for the yaw trailer motion. A vehicle cargo, such as the considered trailer, has its center of gravity at a higher position because of trestles and suspensions. As the trailer motions increased, the tension of the lashing wires increased simultaneously, causing larger trailer motions. The location of the center of gravity was assumed to be the same as its initial position. However, the center of gravity of the loaded cargo could shift from its position inside the trailer in the case of excessive trailer motion. To reproduce the accidents of collapsed trailers this assumption is discussed in Section 5.2.

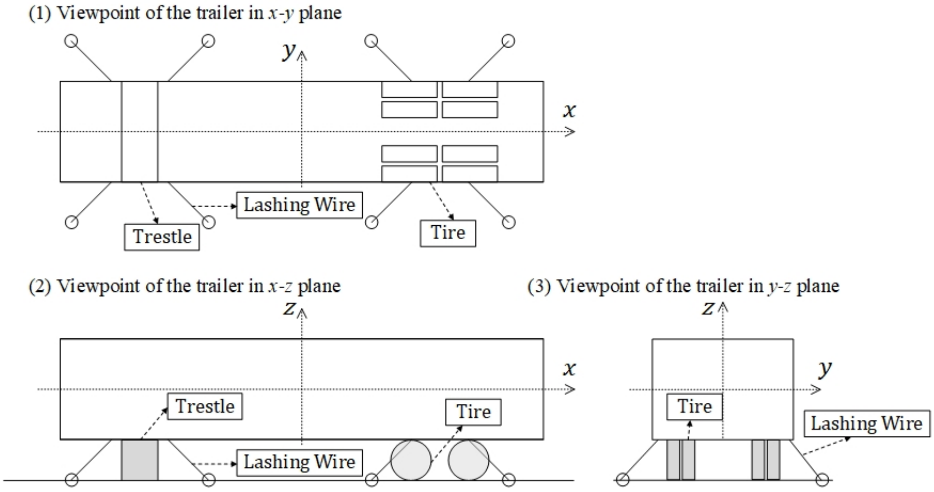

Figure 5 Symmetrical lashing arrangement of a trailer

To analyze the trailer motions, all external forces acting on the trailer must be checked. The centrifugal and tangential forces are generated by the ship motions, which can cause the trailer motions. Figure 6 shows the forces on the lashed trailer due to the ship roll and pitch motions. In Figure 6, the centrifugal force is shown in the red color, and the tangential force in blue. The gravity force is marked in green, which exists even if ship motions do not occur.

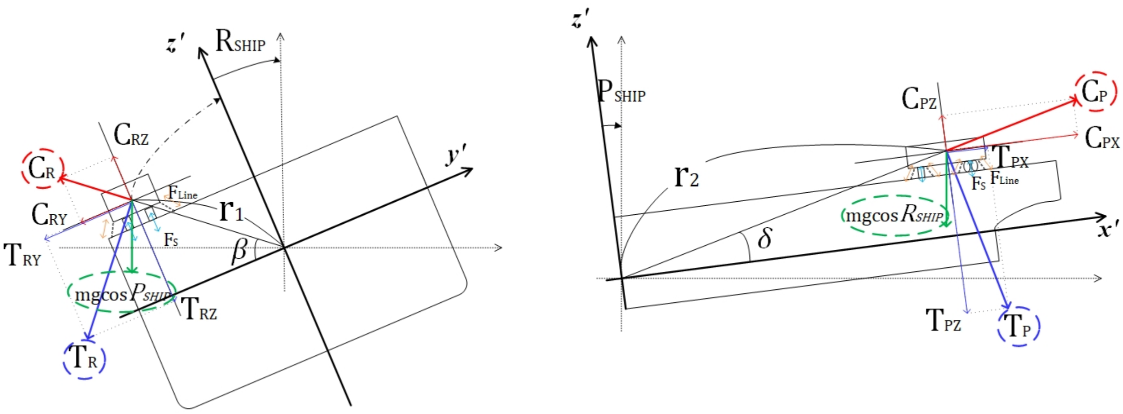

(a) Forces by ship roll motion in the y'-z' plane **(b) Forces by ship pitch motion in the x'-z' plane**

Figure 6 Various forces on trailer caused by ship roll and pitch motions

Figure 6 (a) shows the centrifugal and tangential forces caused by the ship roll motion. They are expressed as follows.

$$T_{Ry} = mr_1\ddot{R}_{SHIP}\sin\beta, \tag{11}$$

$$T_{Rz} = mr_1\ddot{R}_{SHIP}\cos\beta, \tag{12}$$

$$C_{Ry} = mr_1(\dot{R}_{SHIP})^2\cos\beta, \tag{13}$$

$$C_{Rz} = mr_1(\dot{R}_{SHIP})^2\sin\beta, \tag{14}$$

where T_{Ry} and T_{Rz} are the tangential forces and C_{Ry} and C_{Rz} are the centrifugal forces due to the ship roll motion along the *y*- and *z*-axes, respectively. m is the mass of the trailer, r_1 is the distance between the centers of the ship and trailer in the y-z plane, and R_{SHIP} is the angle of the ship roll motion. β is the angle between the centers of the ship and trailer in the y-z plane.

Figure 6 (b) shows the centrifugal and tangential forces caused by the ship pitch motion. They are expressed as follows.

$$T_{Pz} = mr_2\ddot{P}_{SHIP}\cos\delta, \tag{15}$$

$$T_{Px} = mr_2\ddot{P}_{SHIP}\sin\delta, \tag{16}$$

$$C_{Pz} = mr_2(\dot{P}_{SHIP})^2\sin\delta, \tag{17}$$

$$C_{Px} = mr_2(\dot{P}_{SHIP})^2\cos\delta, \tag{18}$$

where T_{Px} and T_{Pz} are the tangential forces and C_{Px} and C_{Pz} are the centrifugal forces due to the ship pitch motion in the x- and z-axes, respectively. r_2 is the distance from the center of gravity of the ship to the center of the trailer in the x-z plane. P_{SHIP} is the angle of the ship pitch motion, while δ is the angle between the center of gravity of the ship and the center of the trailer in the x-z plane. By including these forces, the five modes of the trailer motions are expressed according to the following equations.

$$f_x(x,y,z,R_T,P_T) = m\ddot{x} = mg\cos R_{SHIP}\sin P_{SHIP} - T_{Px} - C_{Px} - (F_{LX}+F_{RX}) - F_S\mu_S\,\mathrm{sign}(\dot{x})\ , \tag{19}$$

$$f_y(x,y,z,R_T,P_T) = m\ddot{y} = -mg\cos P_{SHIP}\sin R_{SHIP} - T_{Ry} - C_{Ry} + (F_{LY}-F_{RY}) - F_S\mu_S\,\mathrm{sign}(\dot{y})\ , \tag{20}$$

$$f_z(x,y,z,R_T,P_T) = m\ddot{z} = mg\cos R_{SHIP}\cos P_{SHIP} + (T_{Pz}+T_{Rz}) - (C_{Pz}+C_{Rz}) - (F_{LZ}+F_{Rz}) - F_S\ , \tag{21}$$

$$f_{Roll}(x,y,z,R_T,P_T) = I_{Roll}\ddot{R_T} = F_{RY}[Z_R\cos R_T\cos P_T - B_R\sin R_T] - F_{LY}[Z_L\cos R_T\cos P_T + B_L\sin R_T] - F_{RZ}[Z_R\sin R_T\cos P_T + B_R\cos R_T] + F_{LZ}[-Z_L\sin R_T\cos P_T + B_L\cos R_T] - F_{SR}[(Z_G+Z_{SS})\sin R_T\cos P_T + B_S\cos R_T] + F_{SL}[-(Z_G+Z_{SS})\sin R_T\cos P_T + B_S\cos R_T] - F_S\mu_S(Z_G+Z_{SS})\,\mathrm{sign}(\dot{y}), \tag{22}$$

$$f_{Pitch}(x,y,z,R_T,P_T) = I_{Pitch}\ddot{P_T} = \sum_{i=1}^{4}\{F_{LX(i)}[Z_{L(i)}\cos R_T + X_{L(i)}\sin P_T] + F_{RX(i)}[Z_{R(i)}\cos R_T + X_{R(i)}\sin P_T] - F_{LZ(i)}[X_{L(i)}(1-\cos P_T) - Z_{L(i)}\cos R_T\cos P_T] - F_{RZ(i)}[X_{R(i)}(1-\cos P_T) - Z_{R(i)}\cos R_T\cos P_T]\} + \sum_{i=1}^{4}\{mg\cos R_{SHIP}\cos P_{SHIP}\,[X_{L(i)}(1-\sin P_T) - Z_G\cos R_T\sin P_T] + mg\cos R_{SHIP}\sin P_{SHIP}\,[X_{L(i)}\sin P_T + Z_G\cos R_T\cos P_T]\} + \sum_{i=1}^{2}\{F_S[X_S\cos P_T + Z_{SS}\cos R_T\sin P_T]\}, \tag{23}$$

where I_{Roll} and I_{Pitch} are the inertial moments of the trailer under the roll and pitch motions of ship, respectively, and f_x, f_y, f_z, f_{Roll}, and f_{Pitch} are the forces acting on the trailer under the surge, sway, heave, roll, and pitch modes of trailer, respectively. F_{LX}, F_{LY}, F_{LZ}, F_{RX}, F_{RY}, and F_{RZ} are the horizontal, lateral, and vertical forces acting on the lashing wire on the left and right sides, respectively. F_S and μ_S are the load and friction coefficients for the suspension, respectively. Z_L and Z_R are the vertical distances between the spar and spine on the left and right sides, respectively, and Z_G and Z_{SS} are the vertical distances between the mass and spine, and between the top of the suspension and spine, respectively. B_L and B_R are the width of the trailer at the lashing wire on the left and right sides, respectively, and B_S is the half-width of the trailer body at the suspension. X_L and X_R are the horizontal distances between the lashing point and longitudinal center of gravity on the left and right sides, respectively. X_S is the horizontal distance of the suspension from its longitudinal center of gravity.

The equations of motion and momentum for the trailer can be expressed by simultaneous equations, as

$$\begin{bmatrix} m & 0 & 0 & 0 & 0 \\ 0 & m & 0 & 0 & 0 \\ 0 & 0 & m & 0 & 0 \\ 0 & 0 & 0 & I_{Roll} & 0 \\ 0 & 0 & 0 & 0 & I_{Pitch} \end{bmatrix} \begin{bmatrix} \ddot{x} \\ \ddot{y} \\ \ddot{z} \\ \ddot{R}_T \\ \ddot{P}_T \end{bmatrix} = \begin{bmatrix} f_x(x,y,z,R_T,P_T) \\ f_y(x,y,z,R_T,P_T) \\ f_z(x,y,z,R_T,P_T) \\ f_{Roll}(x,y,z,R_T,P_T) \\ f_{Pitch}(x,y,z,R_T,P_T) \end{bmatrix} , \tag{24}$$

Eq. (24) is numerically solved owing to the strong dynamic nonlinearity. The time interval is very important for maintaining accuracy. However, the computation did not converge at a constant time step, as in the fourth order Runge-Kutta method. The Runge-Kutta Merson method (Burgin, 1970) adjusted the value of the time interval, as it monitored the numerical error at every time step. The initial time interval of the simulation was defined as 0.001 s, which was halved when the numerical error was larger than the admissible value. Every time length of the time-domain analysis was defined as 1,200 s. The amplitude of the trailer motions was statistically processed as a significant value using the zero-up-crossing method.

Each force occurring on the suspension and wire has already been shown in former studies (Turnbull and Dawson, 1994, 1997 and 1999; Turnbull, 2000; Poulios et al., 2008 and 2009). However, some mistakes in these formulas were found by the authors. These formulas are summarized again, and only the equations are described here. The definition of each variable is provided in the appendix, please see the definition of each force in Poulios et al. (2008 and 2009).

$$F_{SL,R} = K_S[Z_H - (Z_G + Z_{SS})\cos R_T \cos P_T \mp B_S \sin R_T \cos P_T - X_S \sin P_T - Z_S] + \lambda_S[\dot{Z}_H + (Z_G + Z_{SS})\dot{R}_T \sin R_T \cos P_T + (Z_G + Z_{SS})\dot{P}_T \cos R_T \sin P_T \pm B_S\dot{R}_T \cos R_T \cos P_T \mp B_S\dot{P}_T \sin R_T \sin \dot{P}_T - X_S\dot{P}_T \cos P_T] , \tag{25}$$

$$F_{Line} = K_{Line}(L_{Li} - L_0) , \tag{26}$$

$$L_{Li} = \sqrt{{S_{Li}}^2 + {T_{Li}}^2 + {C_{Li}}^2} , \tag{27}$$

$$S_{Li} = A_{L(i)} + y_{(i)} + Z_{L(i)} \sin R_T - B_{L(i)} \cos R_T , \tag{28}$$

$$T_{Li} = z_{(i)} - Z_G \cos R_T - Z_{L(i)} \cos R_T - B_{L(i)} \sin R_T - X_{L(i)} \sin P_T , \tag{29}$$

$$C_{L1} = x_{(1)} - 0.5 - Z_{L(1)} \sin P_T - X_{L(1)}(1 - \cos P_T), \tag{30}$$

$$C_{L2} = x_{(2)} + 0.5 - Z_{L(2)} \sin P_T - X_{L(2)}(1 - \cos P_T) , \tag{31}$$

$$C_{L3} = x_{(3)} - 0.5 + Z_{L(3)} \sin P_T + X_{L(3)}(1 - \cos P_T) , \tag{32}$$

$$C_{L4} = x_{(4)} + 0.5 + Z_{L(4)} \sin P_T + X_{L(4)}(1 - \cos P_T) , \tag{33}$$

$$F_{LXi} = F_{Li}\frac{C_{Li}}{L_{Li}} , \tag{34}$$

$$F_{LYi} = F_{Li}\frac{S_{Li}}{L_{Li}} , \tag{35}$$

$$F_{LZi} = F_{Li}\frac{T_{Li}}{L_{Li}} , \tag{36}$$

Several main assumptions were required for this study. First, the rotational ship motions such as roll and pitch were assumed to influence to the lashed trailer motions. The horizontal and vertical ship motions were assumed to not contribute to the trailer motions. The rudder force and moment were not taken into account, because the detail of rudder use was unavailable. Therefore, the five modes of trailer motions were caused by the two modes of ship motions. Second, there are many studies on nonlinear ship motions, such as the parametric roll resonance (Acanfora et al., 2017a and 2017b). However, this was not considered because the parametric roll resonance usually occurs in the head sea and the wave conditions for this study approximate beam sea conditions. The selected target ship is a domestic ferry, which has a different shape to that of a container ship. The nonlinear wave exciting forces were not considered in the seakeeping model, EUT. On the other hand, the WW3 model includes both linear and nonlinear source terms. The nonlinear wave–wave interaction terms are considered in the open water, the detail of which is described in the technical note (Tolman, 2014). For the lashed trailer motions, the nonlinear angular velocity is considered using only the centrifugal force, and the mooring forces due to the wire rope can be regarded as linear owing to the force–elongation property of the rope.

4. Simulation cases and results for a trailer accident in rough sea

The conditions of trailer and ferry for the numerical simulations are described in Section 4.1. A serious cargo collapse accident was simulated, including the offshore waves and ship and trailer motions. Section 4.2 summarizes the weather conditions for the case studies. Section 4.3 presents the simulated results of the ship motions, and Section 4.4 describes the lashed trailer motions required to reproduce the reported collapse of 100 trailers.

4.1 Conditions of loading trailers on ferries

Numerical simulations were conducted for the Ferry D belonging to the ferry company. The primary dimensions are listed in Table 1, with a total loading capacity of 154 large trailers. The main specifications for the trailers, suspensions, and lashing wires, as listed in Table 2, were referred to from related studies (Ota et al., 2000; Poulios et al., 2008 and 2009; Abdelkareem et al., 2022). The trailer-loading plan is shown in Figure 7. In this study, the gap between trailers was set to 1.5 m and 1.0 m on the *x*- and *y*-axes, respectively. The 154 trailers were placed in 11 columns, seven rows, and two decks on the *x*-, *y*-, and *z*-axes, respectively.

Table 1 Primary dimensions of Ferry D

Length, overall	190.0 m
Length, between perpendiculars	175.0 m
Breadth	26.4 m
Draft (fully loaded)	6.85 m
Displacement (fully loaded)	15,843 t
Metacentric height	2.3 m
Voyage speed	25.0 knots

Table 2 Main specification of trailers, suspensions, and lashing wires

Length	12.0 m
Width	2.5 m
Height of center of gravity	1.85 m
Weight	20.0 t
Suspension spring stiffness coefficient	26 kN/m
Suspension damping coefficient	520 N s/m
Lashing wire spring stiffness coefficient	318.5 kN/m

As mentioned in Section 3.3, the force acting on the trailer can be different for the position of each trailer. Particularly, the centrifugal and tangential forces may increase as the position of the trailer gets farther away from the center of gravity of the ship. Thus, the total force and motion of the trailer, located at the outermost section, are expected to be of most significance. In this study, the equations of motion were analyzed for all trailers to compare the differences in trailer motion and lashing wire tension.

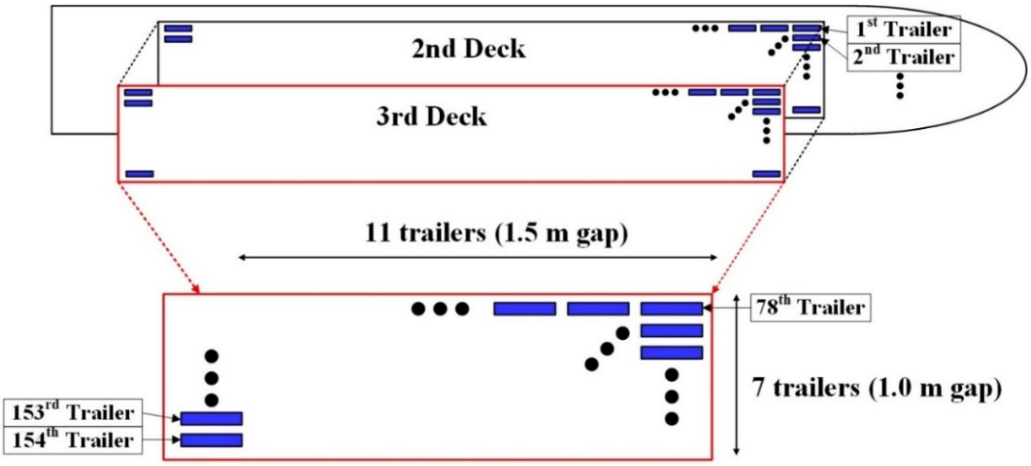

Figure 7 Trailer-loading position on Ferry D

4.2 Weather conditions and simulated results of waves

Numerical simulations were conducted for two cases, as listed in Table 3. In this study, the collapse accident of loaded trailers in the Japanese domestic Ferry D, which was described in Section 2, was numerically reproduced to analyze the parameters that lead to the accident. The accident occurred during the voyage of April 26, 2009, from O Port to T Port. The variations in the weather chart for April 24 to 27, 2009 are summarized in Figure 8.

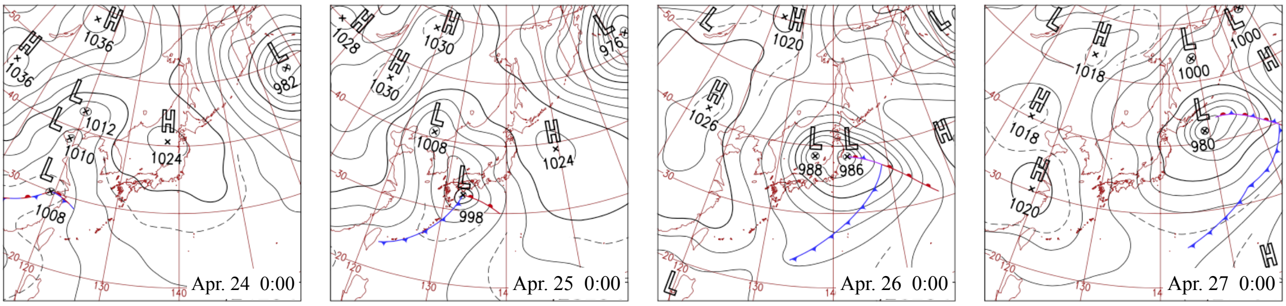

Figure 8 Variations in the weather chart of April 24 to 27, 2009

Low pressure is known to develop rapidly as it moves northeasterly. Although the development of low pressure was forecasted beforehand, the strength was significantly underestimated. Thus, resulting in one of the typical failed forecast patterns for developing low-pressure systems. In Case 1, the situation of the ship and trailers was reproduced on the day before the accident for comparison with that in Case 2, where a detailed situation of the trailers and ferry was numerically simulated in rough weather in an actual sea. Table 3 summarizes the period, location, and wave height for Cases 1–2. Time is shown as the universal time coordinated (UTC).

Table 3 Case studies for trailer lashing model of ferry

	Date and time	Depart from	Arrive at	H_S (m)	Remarks
Case 1	2009.04.24 16:30 – 04.25 10:45	T Port (Hokkaido)	O Port (Kanto)	2.5	One day before the accident
Case 2	2009.04.25 16:30 – 04.26 12:00	O Port (Kanto)	T Port (Hokkaido)	9.0	Accident Occurrence Day

For Cases 1 and 2, a trailer collapse accident, which occurred on April 26, 2009, was reproduced. As speculated, the accident may have occurred mainly due to the underestimation of the low-pressure strength in weather forecasts. A ferry company usually makes decisions on its operations from weather forecast results, 24–48 h before departure. However, the accuracy of a weather forecast remains insufficient (Natskår et al., 2015; Girolamo et al., 2017; Chen and Wang, 2020; Chen et al., 2020; Lee et al., 2021 and 2022).

(1) Case 1

The simulated wave height distributions with wind vectors in Case 1 are shown in Figure 9. The existence of rough waves was not observed during the voyage from T Port to O Port. However, rough waves of approximately 3 m were seen 1–3 h before the arrival at O Port (11:00, April 25, 2009). If the arrival of the ferry was delayed by a couple of hours, operational difficulties could have occurred. Thus, rough waves develop with increased wave heights over the voyage on the next day, leading to accidents. In Figure 9, high waves can be seen in the Pacific Ocean near Japan in the morning of April 25. Large wind vectors are located in the same area; thus, we should consider the influence of wind waves on the ferry.

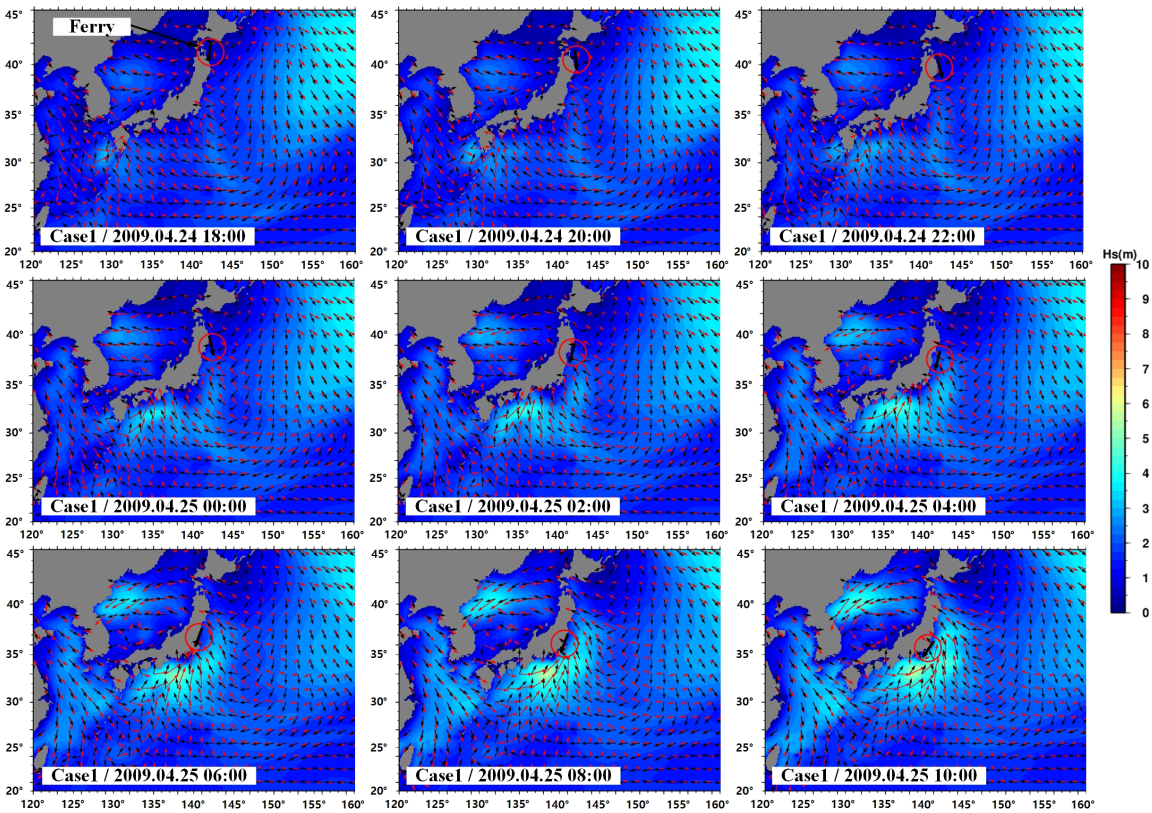

Figure 9 Variation in simulated wave height distributions with wind vectors for Case 1

Figure 10 shows variations in weather parameters from the NOWPHAS and WW3 simulated results in each ship position. Wave data was not available in the NOWPHAS for 1 h between 5:00 and 6:00 on April 25, 2009 and is marked by a red shading. A comparison of the NOWPHAS with the WW3 simulations resulted in relatively similar observation for Case 1. Thus, a wave height of approximately 2 m can be estimated between 5:00 and 6:00 from the simulated results of WW3. Variations in the ship speed and heading observed for Case 1 are shown in Figure 11, and the information were obtained from the AIS data. The relative wave direction and encounter frequency are necessary for the seakeeping simulation. Thus, the relative wave direction was known to be approximately 60°, which means the bow quarter or beam seas at that time.

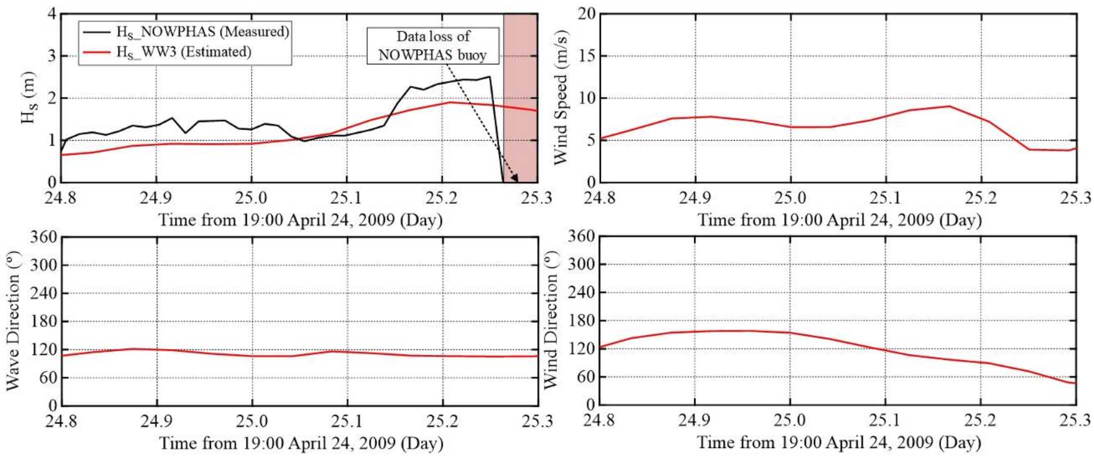

Figure 10 Variation in the weather parameters for Case 1

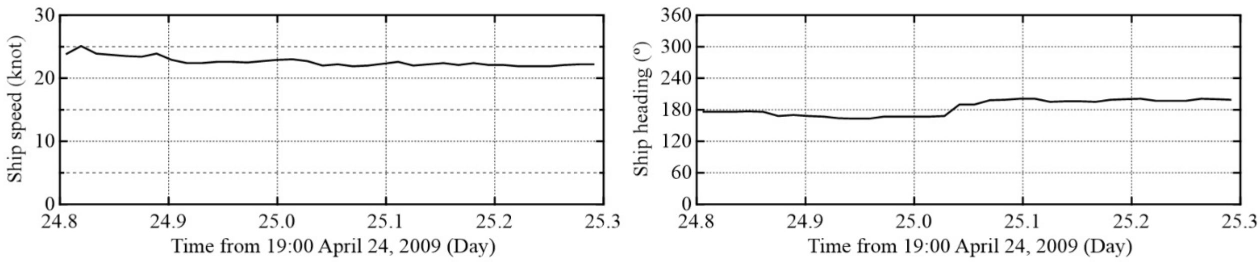

Figure 11 Variation in the ship speed and heading for Case 1

(2) Case 2

On April 26, 2009, the day of the accident, low pressure had increasingly developed on the east coast of the Pacific Ocean in Japan. The simulated wave height distributions with the wind vectors in Case 2 are shown in Figure 12. As shown in Figure 12, the existence of rough waves of height 6–8 m, near the location of the ferry, was obvious from 6:00 to 10:00. The ferry has been near the center of developed atmospheric pressure with swirling winds. Figure 12 also shows that the strong wind from SE direction prevails, and the wave direction is almost similar to that of winds. This may cause very strong waves with nearly the beam sea condition. The ferry in Section 2 was not usually operated in these rough wave conditions. Thus, the weather forecast at that time would have been underestimated, causing the ferry to face a very dangerous situation. Furthermore, the wind speed reached approximately 30 m/s, as shown in Figure 13. Therefore, the ferry encountered a violent wind, equivalent to Level 11 on the Beaufort scale. Figure 14 shows the variations in ship speed and heading on the day of the accident. The relative wave direction was estimated as 60°–90°, which is the bow quarter of the beam sea. Thus, a critical roll motion in the ferry may occur. NOWPHAS lacked data from 7:00–11:00 which is marked by red shading in Figure 13. The period of data loss included the maximum wave height and the situation of the ferry was estimated only by the simulated results of WW3.

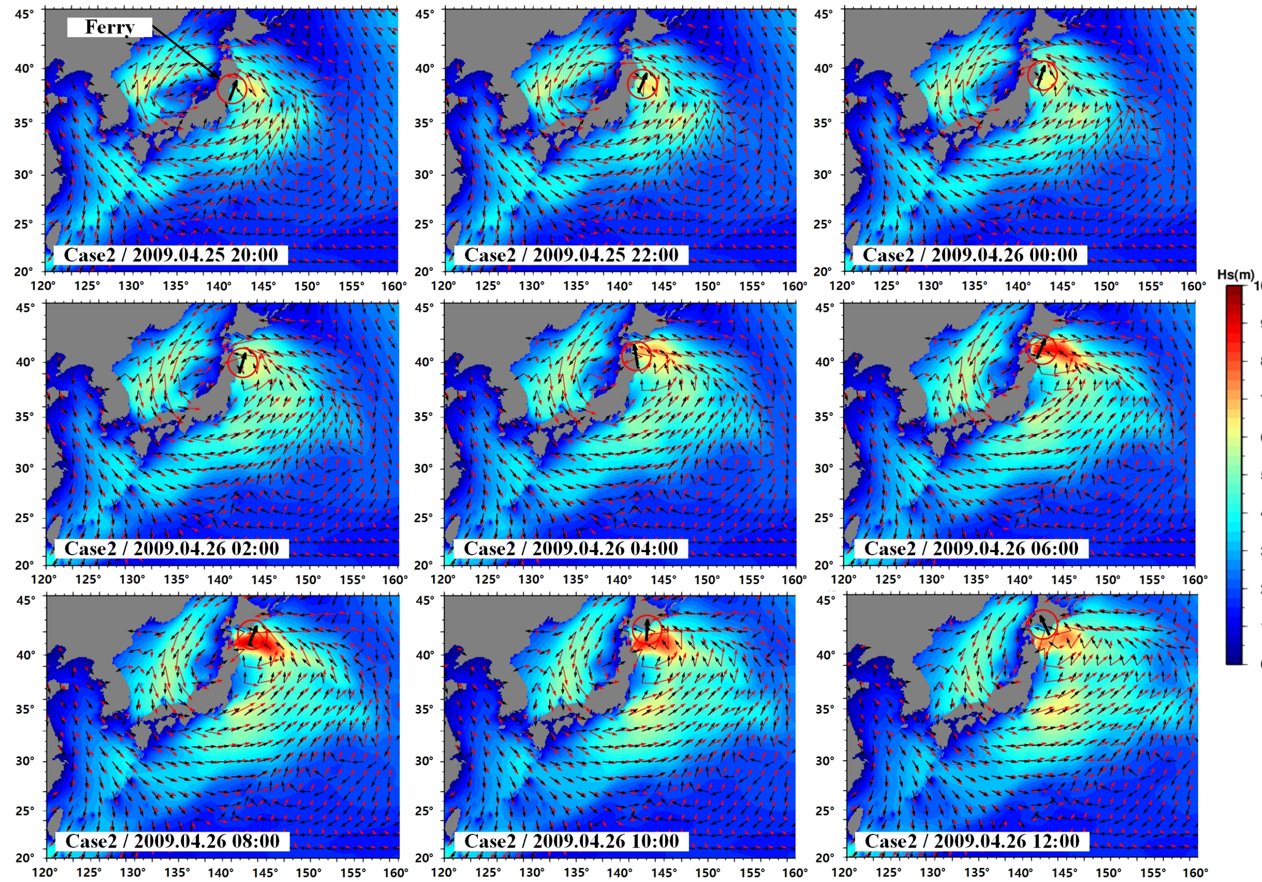

Figure 12 Variation of simulated wave height distributions with wind vectors for Case 2

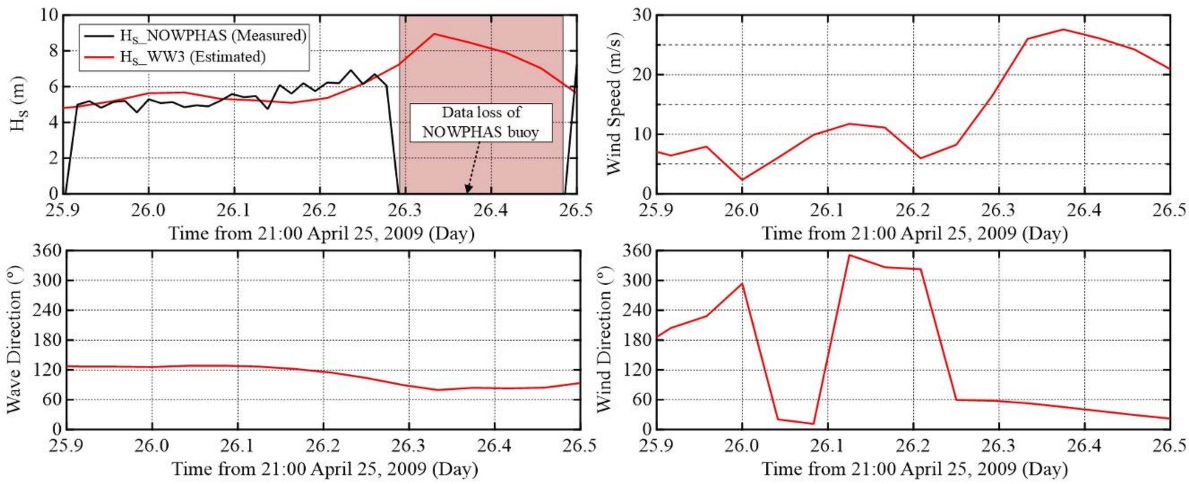

Figure 13 Variation in the weather parameters for Case 2

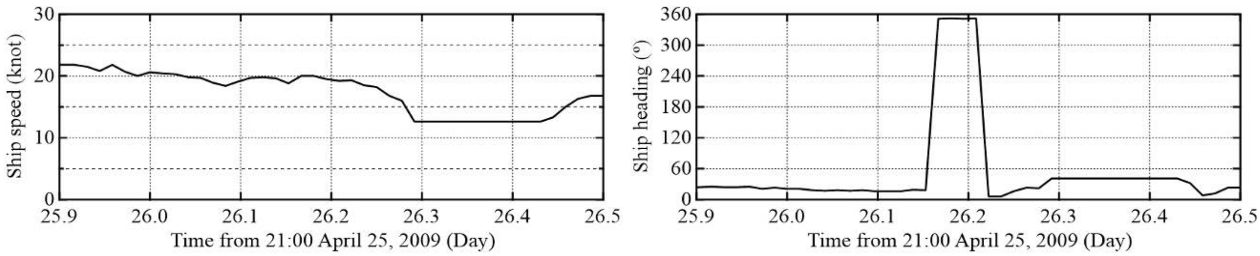

Figure 14 Variation in the ship speed and heading for Case 2

4.3 Simulated results for ship motions

The wave directional spectrum approximated by the NOWPHAS system and that estimated by WW3 were used to reproduce the ship motions using the EUT. Similarly, the ship motions could be predicted without significant differences, using the two data sources. The ship roll and pitch motions were obtained with time length defined as 1,200 s by Eqs. (9) and (10). Figure 15 shows the time series of the estimated ship roll and pitch motions from 05:00 to 05:20 April 26, 2009.

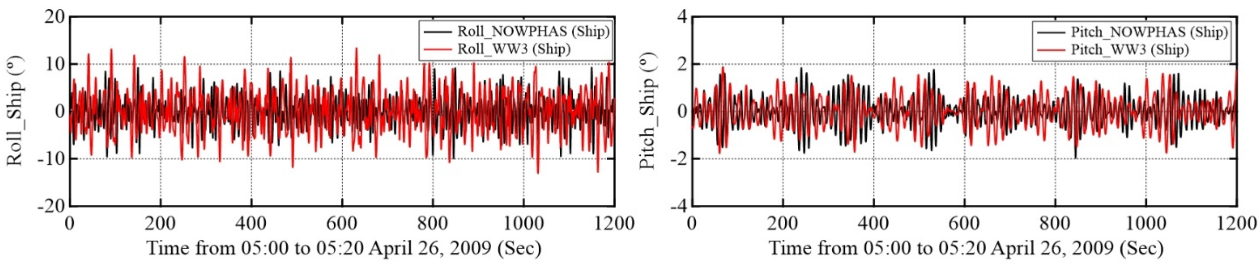

Figure 15 Time series of the estimated ship roll and pitch motions from 05:00 to 05:20 April 26, 2009

Based on the weather conditions for Cases 1 and 2, the ship motions were reproduced using the EUT, as shown in Figures 16 and 17. In Case 1, the pitch motion was relatively weak at approximately 1°. However, the roll motion reached approximately 13° because rough waves of approximately 3 m were affected by the beam sea direction. Under such wave directions, a ferry can cause significant roll motion; thus causing large trailer motions. However, the waves were not sufficiently harsh to cause special problems during the voyage.

In Case 2, the ferry was directly affected by very rough waves of approximately 5–9 m. Owing to the shape of the ferry, which had a narrow width and long length, roll motion could occur very critically under the beam sea direction. As shown in Figure 13, the wave height observed in the NOWPHAS buoy was approximately 6 m, and the wave height estimated by WW3 was approximately 9 m. Thus, pitch motion occurred at approximately 5°, while roll motion reached approximately 30–40°. Although the results appear to overestimate the roll motion, 9 m of rough waves can have a fatal effect on the ferry operations.

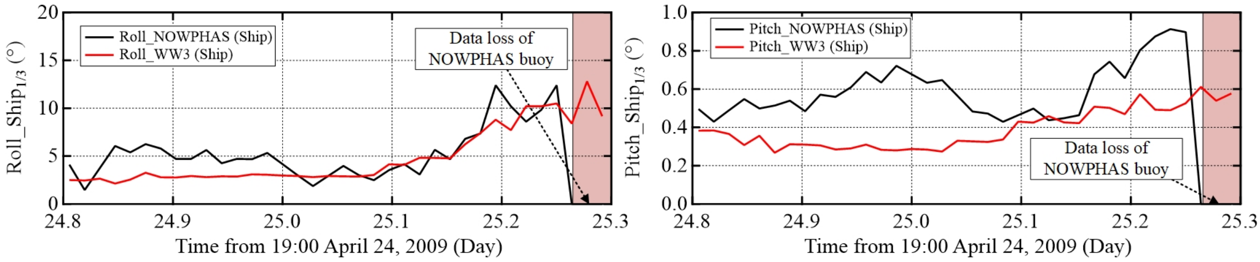

Figure 16 Variation in the estimated ship roll and pitch motions for Case 1

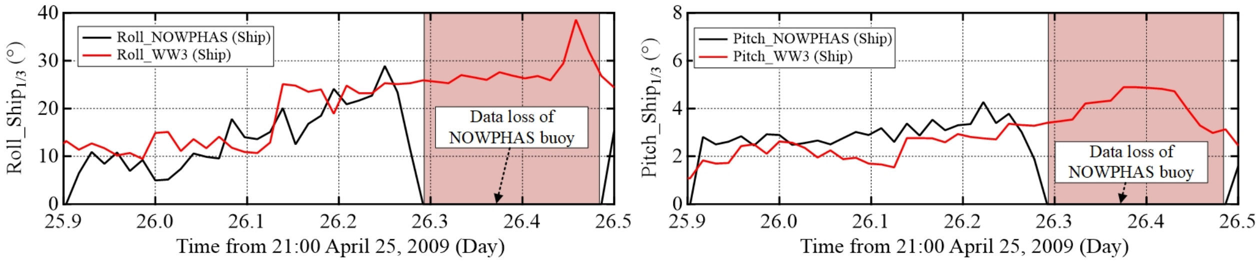

Figure 17 Variation in the estimated ship roll and pitch motions for Case 2

In Section 4.1, 4.2 and 4.3, the simulation conditions of the trailer lashing model were described, including the weather conditions and estimated ship motions. Theoretically, the trailer inside the ferry could be exposed to various forces causing the trailer motions, as discussed in Section 3.3. Thus, trailer motions and lashing wire tensions were studied using the trailer lashing model for a safety evaluation.

4.4 Simulated results of trailer motions and lashing wire tensions

A simulation was conducted to determine the cause of the trailer accident. The trailer motion simulation was conducted for 1,200 s, and the maximum amplitudes for each trailer motion and maximum lashing wire tension were obtained. The example of time series of the simulated trailer motions and lashing wire tension is shown in Figure 18.

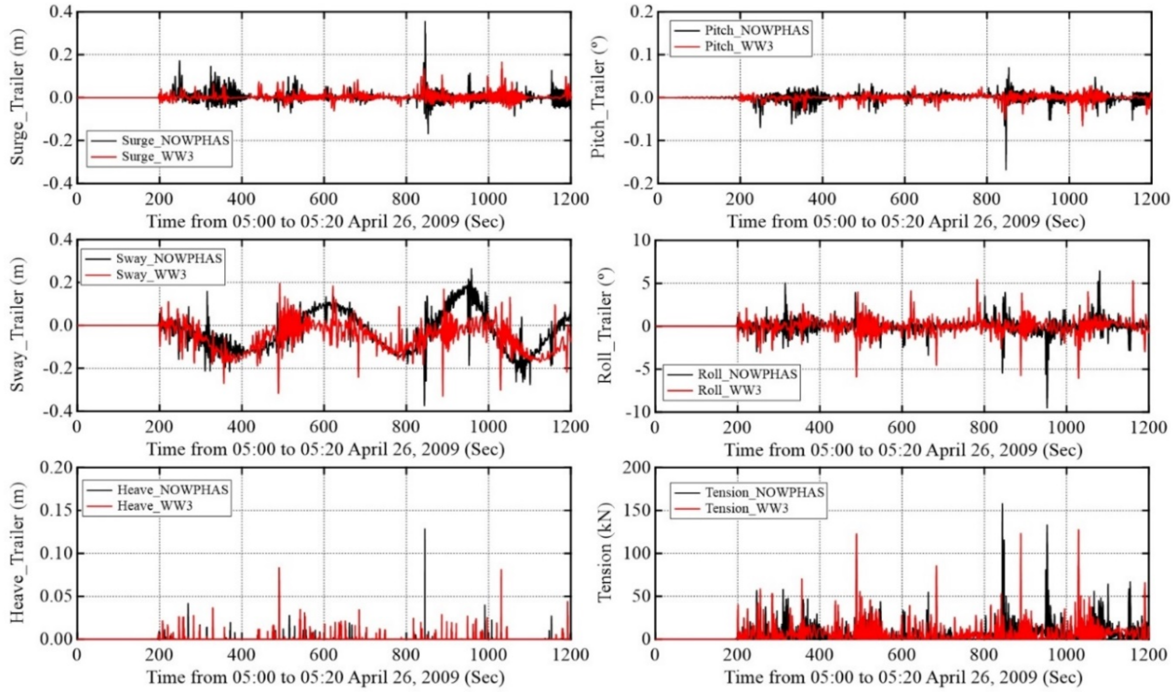

Figure 18 Time series of the simulated trailer motions and lashing wire tension from 05:00 to 05:20 April 26, 2009

In Case 1, the trailer motions were analyzed a day prior to the accident, where the wave height gradually increased to 3 m immediately before entering the O Port, considering which the situations faced by the lashed trailers were reproduced. Figure 19 shows the variations in the simulated trailer motions as the significant value, and maximum tension of the lashing wires obtained from the 20-minute time series in all trailers of the Case 1 simulation.

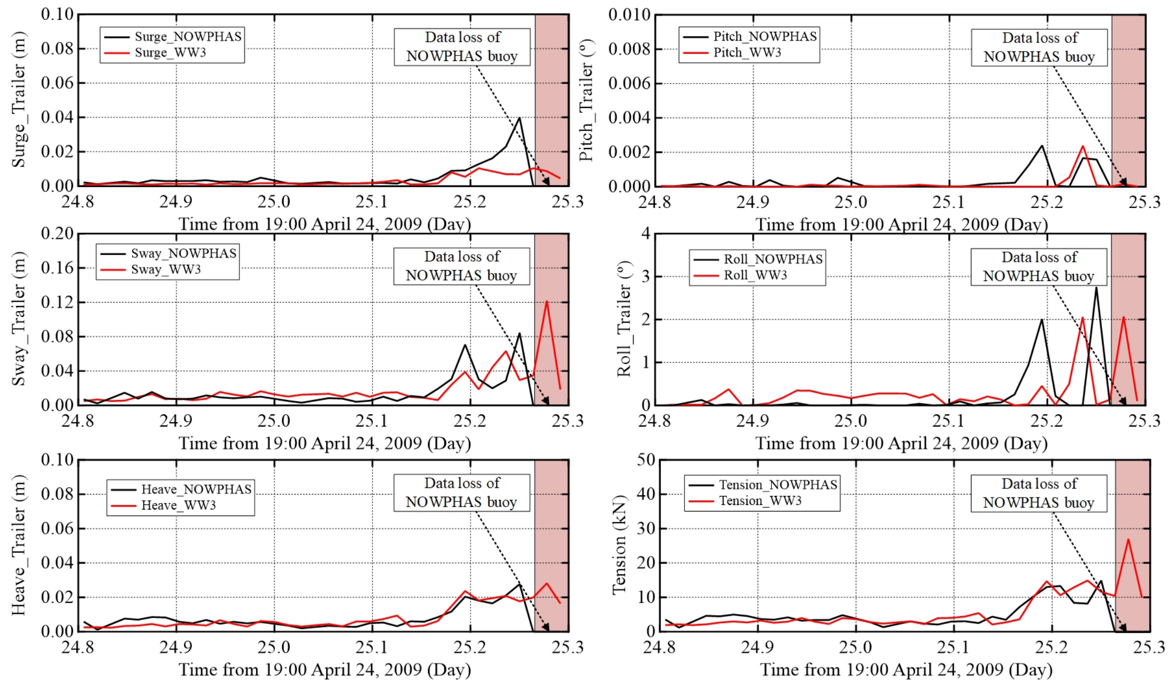

Figure 19 Variation in the simulated trailer motions and lashing wire tension for Case 1

The simulation result of trailer motions shows that surge and heave motions were relatively small, within 0.04 m. However, sway motion was estimated to be approximately 0.12 m. The pitch motion of the trailer was almost zero at 0.002°. Conversely, the roll motion occurred at approximately 3°. For the trailer motion, the lashing wire tension was as small as approximately 30 kN. Thus, no significant problem was expected for the loaded trailer on the day before the accident. The maximum value of each trailer motion and lashing wire tension were compared based on the positions of all the trailers on the cargo deck. The distributions of the maximum motions and lashing wire tensions at the peak time, approximately 26.4 hours from 21:00 on April 25, 2009, are shown in Figure 20. The variations in the trailer motions and the maximum lashing wire tension in Case 2 are shown in Figure 21.

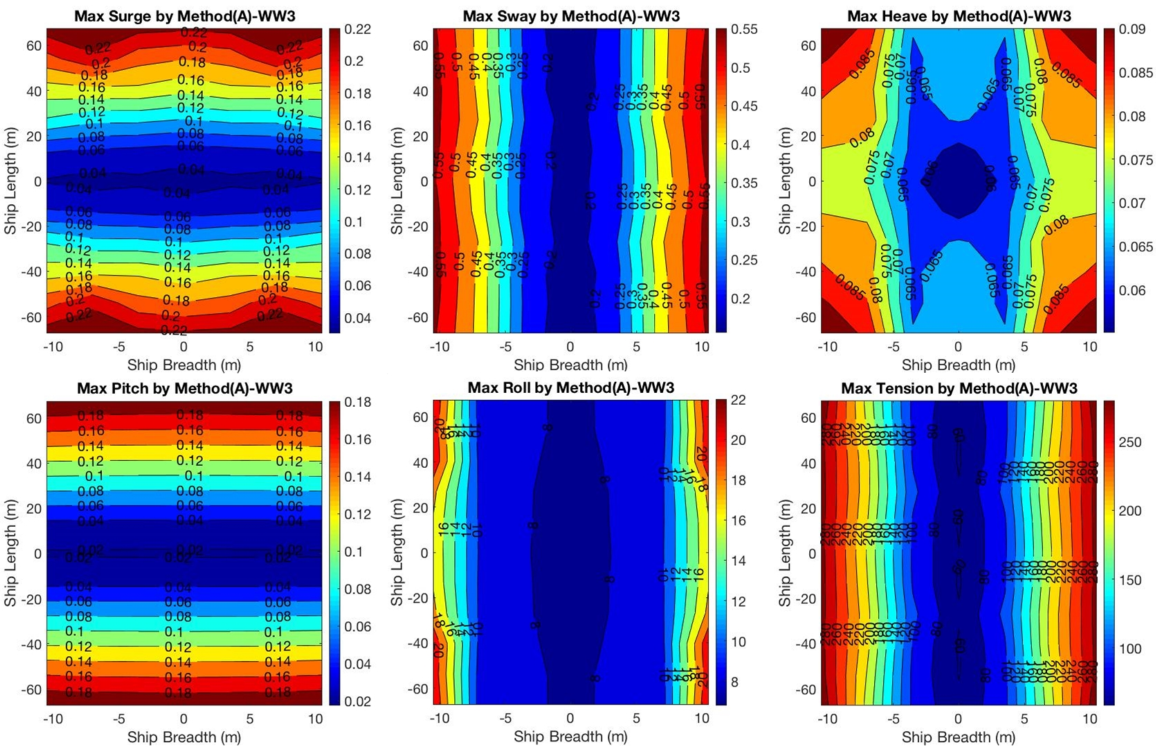

Figure 20 Distributions of various maximum values depending on the trailer position under a rough sea at the peak time

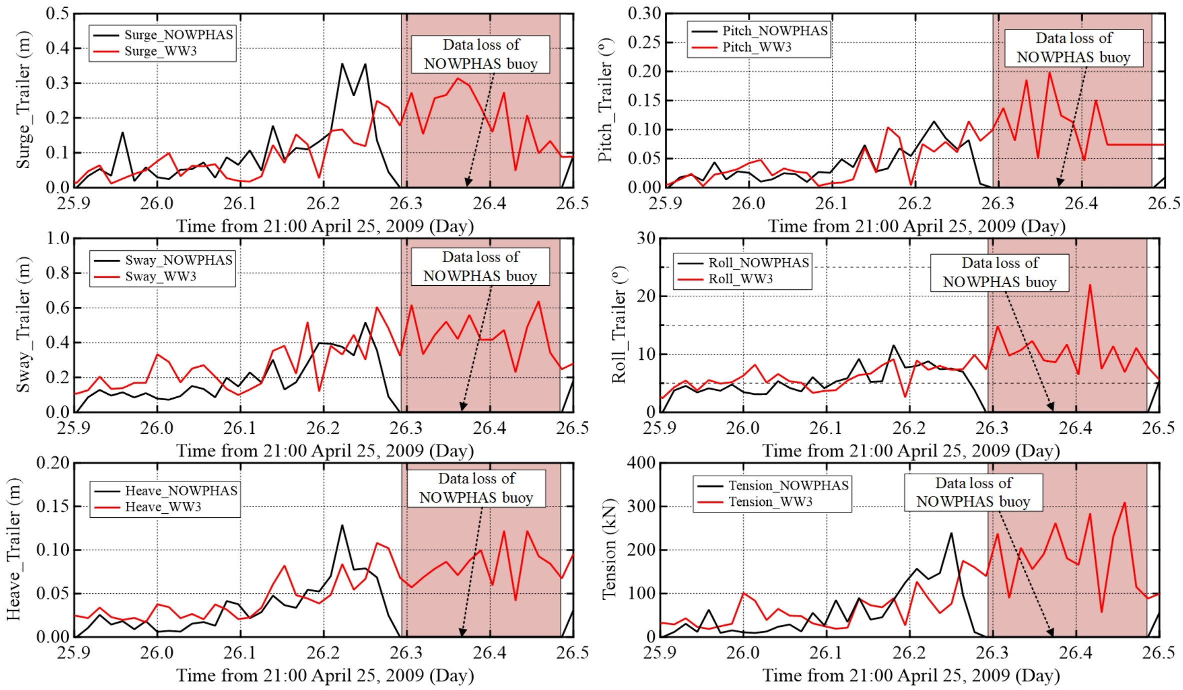

Figure 21 Variation in the simulated trailer motions and lashing wire tension for Case 2

The surge and pitch motions of the trailer were mainly affected by the pitch motion of the ferry, which also generated a force in the longitudinal direction. The results show that the maximum surge motion of the trailer was approximately 0.22 m when trailers were located in the fore and aft sections of the cargo deck. The roll motion of the ferry led to the maximum sway motion of the trailer at approximately 0.55 m in the far left and right corners of the ship. Thus, the closer the position of the trailer to the center of gravity of the ship, the smaller the trailer motions. Conversely, the trailer motions were the largest when the trailer was located on the port and starboard sides. Therefore, the lashing wire tensions increased remarkably to approximately 300 kN, making it difficult to maintain the safety of the trailer lashing. As shown in Figure 17, the estimated roll motion of the ferry reached a maximum of approximately 30°, and when coupled with the large sway motion of the trailer, can lead to a trailer collapse. Furthermore, the trailer motions were predicted to increase, with no trailers loaded in the farthest row of the fore and aft sections. The surge motion reached to 0.35 m, while the heave motion was 0.13 m. Especially, the maximum sway motion reached 0.6 m. Thus, larger trailer motions resulted in a very high lashing wire tension. The roll motion of the trailer was simulated at a maximum of approximately 20°. Thus, the possibility of a collapsing trailer can be, to some degree, predicted during the voyage.

5. Results and discussions

The simulated results showed a larger tension on the lashing wires owing to the larger roll motion of the trailer. However, the results based only on simulations appear insufficient to analyze the accident factors. Additional considerations were made to analyze the factors that lead to the collapsing accidents involving nearly 100 trailers. The trailer motions were compared by changing the lashing arrangement, as discussed in Section 5.1. For repeated accelerations acting on the loaded cargo, a shift of the loaded cargo was reported, whose influence inside the trailer was briefly considered to analyze the collapse of the trailer in Section 5.2.

5.1 Influence on the trailer motions by changing lashing arrangement of wires

The motions of lashed trailers can be significantly influenced by the geometrical lashing arrangement and spring constant of the wires. A case of moored ship motions in waves (Lee et al., 2021) has validated the influence. A typical lashing method maintains 45° in the longitudinal and lateral directions, which is considered while loading as many trailers as possible, in addition to ensuring safety. However, lashing in the lateral direction must be necessarily strengthened to face the large rolling motions of the ship. Practically, lashing arrangements in ferries or vehicle cargo carriers can be altered depending on the exact location of the trailers or vehicles to prepare for optimal stowage on the Ro-Ro decks (Yakabe et al., 2013; Puisa, 2018; Sun et al., 2022). Therefore, simulations were conducted for different lashing arrangements, as shown in Figure 22, where lashing method (A) is an 8-point lashing method typically used to suppress the surge and sway motions of all lashing wires to be dispersed at 45°. Lashing method (B) is a method to reduce the sway motion of the trailer applied at 90°, while lashing method (C) follows the same direction as method (B) but doubles the length of each wire.

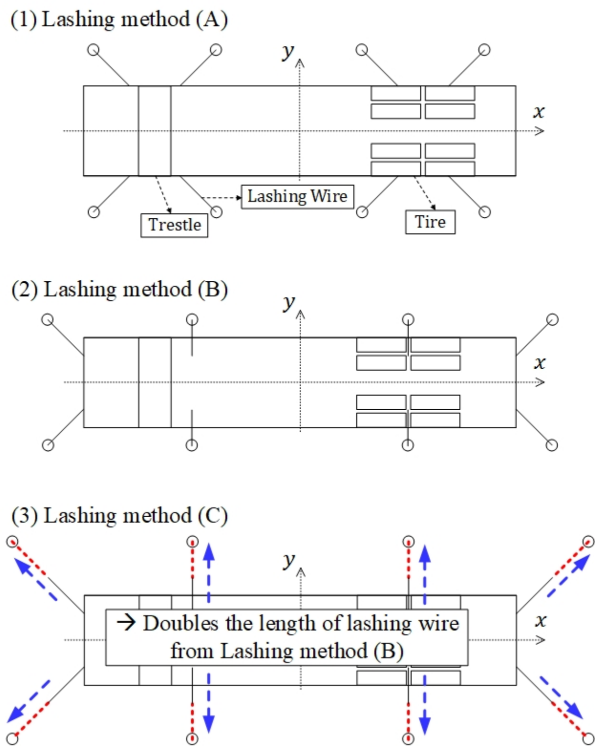

Figure 22 Different types of typical lashing methods for lashed trailer simulations

The previous section showed that the lashing method (A) could not significantly reduce the trailer motions. Thus, the simulation results of changing the lashing wire arrangements using methods (B) and (C) are shown in Figure 23.

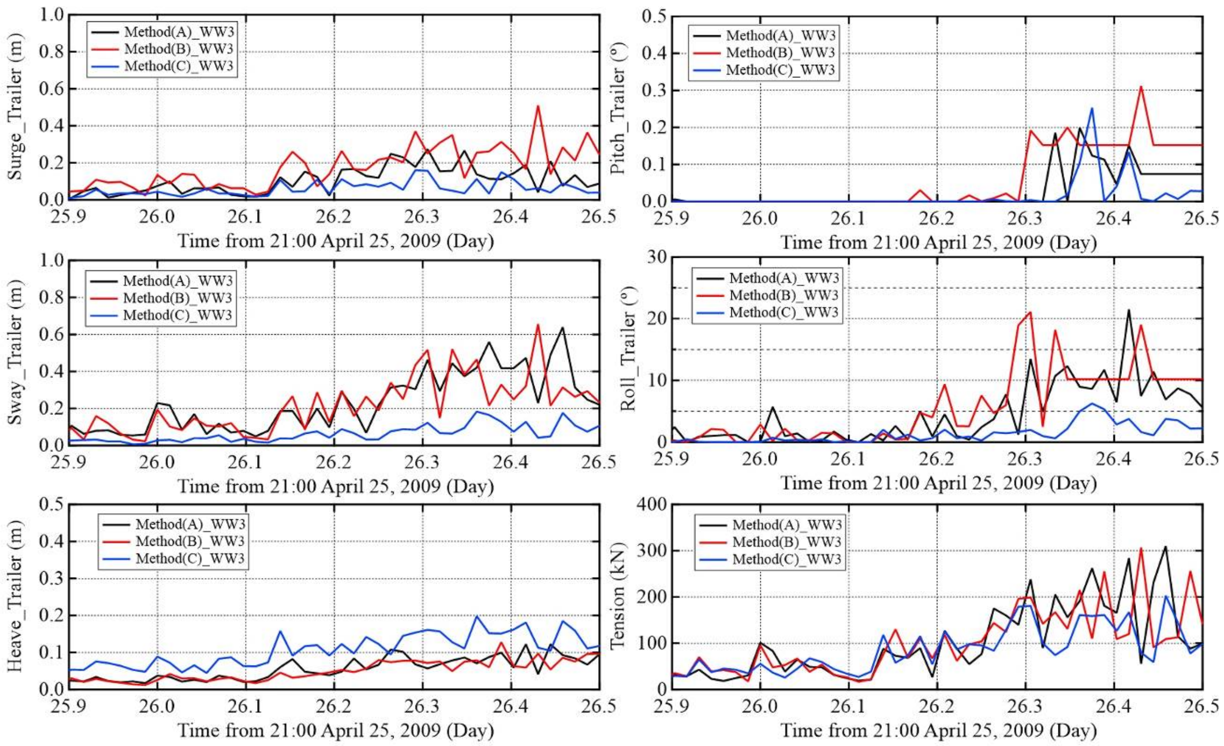

Figure 23 Comparison of the trailer motions and wire tensions for different lashing methods

When methods (A) and (B) were used, the maximum surge motion occurred to approximately 0.4–0.5 m. Conversely, the surge motion was reduced by half to approximately 0.2 m when method (C) was applied. Particularly, the sway motion, which is the most remarkable motion, was expected to be reduced by more than half, from 0.6 m to 0.2 m. The heave motion in method (C) increased from 0.1 m in methods (A) and (B) to 0.2 m. As the length of the lashing wire increased along the horizontal direction, the vertical mooring force became vulnerable to heave motion. The maximum wire tension was nearly 300 kN, which was the breaking limit in methods (A) and (B). Method (C) reduced the wire tension significantly to 200 kN. Thus, method (C) can be effectively used to reduce wire tension and trailer motion, similar to the effect of long breast lines for ship mooring to reduce sway motion (Lee et al., 2021). Longer lashing wires in the longitudinal and lateral directions were thus validated to reduce trailer motions, as in method (C). This method was already demonstrated for the ship mooring of very large crude carriers (VLCC) or liquified natural gas carriers (LNGC) according to the guidelines of the Oil Companies International Marine Forum (OCIMF, 2018). However, the method limits the number of trailers that can be loaded on cargo decks, which can lead to a reduction in profit for ferry companies. Another study can be conducted to optimize safety and profitability by loading the maximum possible number of trailers.

5.2 Shift in the center of gravity of cargos inside trailers

Saito et al. (1996, 1997, 2002) evaluated the possibility of cargo collapse for repeated accelerations in truck transportation. The behaviors of the loaded cargos were measured by experiments under various acceleration patterns. In summary, the filled trailers could easily slip under repeated vibration due to acceleration, especially without lashing. Trailers are secured by lashing wires under the supervision of ferry companies. However, the lashing of cargos inside the trailer is the responsibility of the drivers. Lashing is sometimes difficult when cargos are liquid or raw materials, which may not be lashed rigidly. Thus, the possibility of trailer collapse by shift in the center of gravity of the loaded cargo should be considered. In this study, experimental results were quantitatively applied to cargos inside a trailer on a ferry in an actual sea. A shift of the loaded cargo was assumed due to repetitive motions and accelerations of the trailer. Six patterns of the coordinate shift in the center of gravity were assumed to occur inside the trailer, as shown in Table 4 and Figure 24.

Table 4 Assumed coordinate shift in the center of gravity of cargos inside the trailer

	X (m)	Y (m)
Original	0.0	0.0
S1	2.0	0.0
S2	4.0	0.0
S3	2.0	0.5
S4	4.0	0.5
S5	2.0	1.0
S6	4.0	1.0

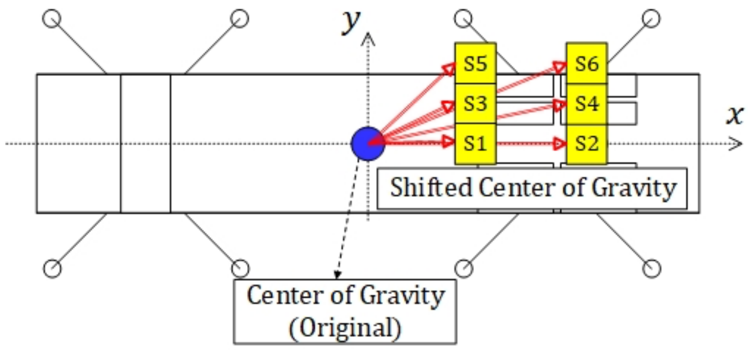

Figure 24 Assumed positions of shifted center of gravity of loaded cargos inside the trailer

The center of gravity was assumed to be shifted by 2 m (Cases S1, S3, and S5) and 4 m (Cases S2, S4, and S6) along the x-axis, while a shift of 0 m (Cases S1 and S2), 0.5 m (Cases S3 and S4), and 1.0 m (Cases S5 and S6) was considered along the y-axis. Numerical simulations of trailer motions were conducted for Case 2, considering the shift in the center of gravity of the loaded cargos for Cases S1–S6. The variations in the simulated trailer motions and maximum lashing wire tensions are summarized in Figure 25.

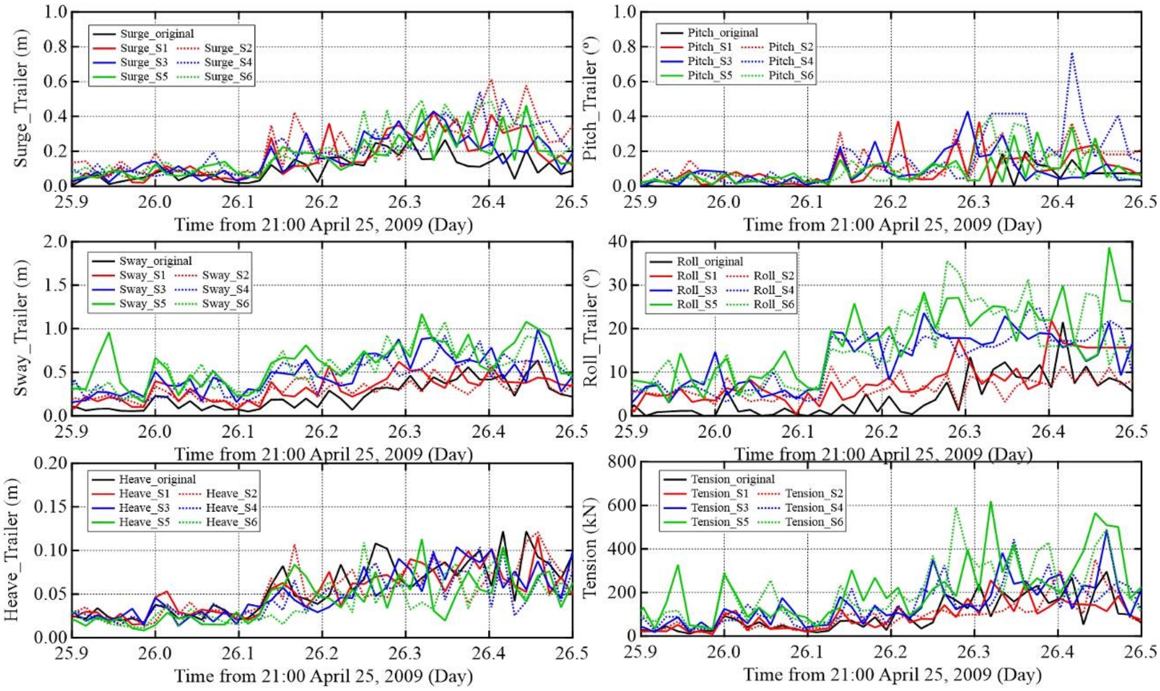

Figure 25 Comparison of trailer motions and lashing wire tensions for center of gravity inside the trailer

The shift in the center of gravity along the *x*-axis was assumed to affect the surge and pitch motions of the trailer, while the shift along the *y*-axis was assumed to affect the sway and roll motions. A surge motion of 0.3 m was observed when no shift was considered. The surge motion was known to increase to 0.5–0.6 m in Cases S2, S4, and S6, while the sway motion increased by approximately 2 times from 0.6 m to 1.2 m in Cases S5 and S6. Particularly, a significant increase in roll motion was estimated from 22° to 38°. Thus, the trailers can easily collapse by losing their balance. Moreover, the lashing wire tension increased by approximately 2 times from 300 kN, without a shift, to 600 kN for Cases S5 and S6. Therefore, the reported situation of 100 trailers that collapsed can be reproduced to some degree considering the simulation results, if the center of gravity of the cargos inside the trailer was shifted in during the rough sea voyage.

6. Conclusions

The safety of cargo and trailer lashing is an essential element to complete shipping operations, especially under rough wave conditions, as the risk of accidents still exists for ferries and Ro-Ro ships in open seas. In this study, numerical models were simulated to evaluate weather conditions, ship motions, and trailer motions. The ship and trailer motions in an irregular sea state were considered in the simulation models. Ship motions were estimated from the wave directional spectrum obtained using NOWPHAS data or WW3 simulated results. Furthermore, a simulation model for trailer motion was developed for irregular ship motion. The model was used to evaluate the behavior of rough waves in actual seas and reproduce the trailer accident that occurred in April 2009, which show that the collapse of trailers might have occurred due to a shift in the center of gravity of cargos inside the trailer, in addition to larger ship motions at maximum wave heights of approximately 9 m. Thus, main conclusions of this study are listed as follows.

(1) A complete simulation model for safety evaluation of a lashed trailer is constructed by the combined analysis of weather conditions, ship motions, and trailer motions, since previous studies did not consider the influence of an irregular sea state, and the evaluation of trailer motions was performed by considering the wave directional spectrum and ship motions. In this study, the time interval in the time-domain analysis of trailer motions was changed to a lower value for convergence. Since the computing time tends to be longer during rough sea conditions, it can be taken as a subject for future research on a practical model.
(2) The sway and roll motions of the lashed trailer were estimated to be dominant. Since the maximum roll motion reached 22°, while the maximum lashing wire tension approached 300 kN under rough waves, it may have caused the trailer to collapse. Following interviews with ferry companies, trailers are not loaded on the fore and aft sections of the ferry under rough waves. However, the port and starboard sides were the most dangerous position of placing trailers, as made obvious by the simulated results, which were different from the experimental ferry operations.
(3) Different lashing arrangements were proposed and compared to verify the effective arrangement applicable to cargo management. Lashing method (C) was validated as the most effective lashing arrangement, where the length of the wires were doubled in the lateral direction to reduce the sway and roll motions of the breast line in VLCC or LNGC terminals. However, the arrangement limits the number of trailers that can be loaded on the cargo deck. Thus, further studies can be conducted to optimize the safety and profitability of ferry operations.
(4) The possibility of shift in cargos inside the trailers must be considered, under repetitive acceleration and motion of the trailer, to show that the risk of trailer collapse increases significantly when a shift occurs in the center of gravity. The shift increased the lateral motions of the trailer by approximately 2 times, which changed the roll motion from 22° to 38°. Thus, the shifted center of gravity inside the trailer may have played a major role in the collapse of the trailers.
(5) In this study, the onboard measurement of the lashed trailer motions on a ferry was not possible for safety reasons. The onboard lashed trailer motions should be used for detailed validation of this model, if such data is available in the future. The model nonlinearities, such as parametric roll resonance, remain as future subjects for consideration. In this study, the shift of the cargo inside the trailer is estimated from the results of land transportation. However, the environment of trailer motions may differ between sea and land operations. Knowledge of the behavior of loaded cargos, such as acceleration and position, is necessary for loaded trailers on ferries or Ro-Ro ships. This can ensure that the evaluation of cargo collapse is more accurate.

Acknowledgments

The authors wish to extend their gratitude toward MOL Ferry Co., Ltd. for their cooperation in conducting the onboard measurements of the 12,000 GT ferry from 2012 to 2015, and allowing valuable interviews. This study was financially supported by Scientific Research (B) (Project No. 22360372, 2010–2012, represented by Kenji Sasa) and Challenging Explanatory Research (Project No. 24651194, 2012–2014, represented by Kenji Sasa) under the Grants-in-Aid for Scientific Research, Japan Society for the Promotion of Science. The authors would like to thank Editage (www.editage.com) for English language editing.

References

Abdelkareem, M. A. A., Zhang, R., Jing, X., Wang, X. and Ali, M. K. A., 2022. Characterization and implementation of a double-sided arm-toothed indirect-drive rotary electromagnetic energy-harvesting shock absorber in a full semi-trailer truck suspension platform. *Energy*, *Vol*.239, 121976. https://doi.org/10.1016/j.energy.2021.121976

Acanfora, M., Montewka, J., Hinz, T. and Matusiak, J., 2017a. On the estimation of the design loads on container stacks due to excessive acceleration in adverse weather conditions. *Marine Structures*, *Vol*.53, pp. 105–123. https://doi.org/10.1016/j.marstruc.2017.01.003

Acanfora, M., Montewka, J., Hinz, T. and Matusiak, J., 2017b. Towards realistic estimation of ship excessive motions in heavy weather. A case study of a containership in the Pacific Ocean. *Ocean Engineering, Vol*.138, pp. 140–150. https://doi.org/10.1016/j.oceaneng.2017.04.025

Booij, N. and Holthuijsen, L. H., 1987. Propagation of ocean waves in discrete spectral wave models. *Journal of Computational Physics*, *Vol*.68, *No*.2, pp. 307–326. https://doi.org/10.1016/0021-9991(87)90060-X.

Burgin, G.H., 1970. Comment on the Runge-Kutta-Merson algorithm. *Simulation, Vol*.15, *No*.2, pp. 89–91. https://doi.org/10.1177/003754977001500219.

Chen, C., Sasa, K., Ohsawa, T., Kashiwagi, M., Prpić-Oršić, J. and Mizojiri, T., 2020. Comparative assessment of NCEP and ECMWF global datasets and numerical approaches on rough sea ship navigation based on numerical simulation and shipboard measurements. *Applied Ocean Research, Vol*.101, 102219. https://doi.org/10.1016/j.apor.2020.102219.

Chen, S. T. and Wang, Y. W., 2020. Improving coastal ocean wave height forecasting during typhoons by using local meteorological and neighboring wave data in support vector regression models. *Journal of Marine Science and Engineering*, *Vol*.8, *No*.3, 149. https://doi.org/10.3390/jmse8030149.

Dee, D. P., Uppala, S. M., Simmons, A. J., Berrisford, P., Poli, P., Kobayashi, S., Andrae, U., Balmaseda, M. A., Balsamo, G., Bauer, P., Bechtold, P., Beljaars, A. C. M., van de Berg, L., Bidlot, J., Bormann, N., Delsol, C., Dragani, R., Fuentes, M., Geer, A. J., Haimberger, L., Healy, S. B., Hersbach, H., Hólm, E. V., Isaksen, L., Kållberg, P., Köhler, M., Matricardi, M., McNally, A. P., Monge-Sanz, B. M., Morcrette, J. –J., Park, B. –K., Peubey, C., de Rosnay, P., Tavolato, C., Thépaut, J. –N. and Vitart, F., 2011. The ERA-Interim reanalysis: configuration and performance of the data assimilation system. *Quarterly Journal of the Royal Meteorological Society*, *Vol*.137, *No*.656, pp. 553–597. https://doi.org/10.1002/qj.828

Girolamo, P. D., Risio, M. D., Beltrami, G. M., Bellotti, G. and Pasquali, D., 2017. The use of wave forecasts for maritime activities safety assessment. *Applied Ocean Research*, *Vol*.62, pp. 18–26. https://doi.org/10.1016/j.apor.2016.11.006.

Grifoll, M. and Martinez de Oses, F. X., 2016. A ship routing system applied at short sea distances. *Journal of Maritime Research*, *Vol*.13, *No*.2, pp. 3–6. ISSN: 1697-4040. https://www.jmr.unican.es/index.php/jmr/article/view/445/487

Grifoll, M., Martorell, L., La Castells, M. and Martinez de Oses, F.X., 2018. Ship weather routing using pathfinding algorithms: the case of Barcelona—Palma de Mallorca. *Transportation Research Procedia*, *Vol*.33, pp. 299–306. https://doi.org/10.1016/j.trpro.2018.10.106

Hughes, D. S. A., 1985. Directional wave spectra using cosine-squared and cosine 2 s spreading functions. *Coastal*

Engineering Technical Note-I-28, *Coastal Engineering Research Center*, *Coastal and hydraulics Laboratory,* U.S. Army Engineer Waterways Experiment Station, Vicksburg, MS.

Ikeda, Y., Fujiwara, T. and Katayama, T., 1993. Roll damping of a sharp-cornered barge and roll control by a new-type stabilizer. *Proceedings of the 3rd International Offshore and Polar Engineering Conference*, Singapore, *Vol*. III, pp. 634-639

Kalnay, E., Kanamitsu, M., Kistler, R., Collins, W., Deaven, D., Gandin, L., Iredell, M., Saha, S., White, G., Woollen, J., Zhu, Y., Chelliah, M., Ebisuzaki, W., Higgins, W., Janowiak, J., Mo, K. C., Ropelewski, C., Wang, J., Leetmaa, A., Reynolds, R., Jenne, R. and Joseph, D., 1996. The NCEP/NCAR 40-year reanalysis project. *Bulletin of the American Meteorology Society*, *Vol.*77, *No.*3, pp. 437–472. https://doi.org/10.1175/1520-0477(1996)077<0437:TNYRP>2.0.CO;2

Kashiwagi, M., 1992. Added resistance, wave-induced steady sway force and yaw moment on an advancing ship. *Ship Technology Research (Schiffstechnik)*, *Vol.*39, pp. 3–16. ISSN: 0937-7255

Kashiwagi, M., 1997. Numerical seakeeping calculations based on the slender ship theory. *Ship Technology Research (Schiffstechnik)*, *Vol*.4, *No*.4, pp. 167–192. ISSN: 0937-7255

Kashiwagi, M., Sugimoto, K., Ueda, T., Yamasaki, K., Arihama, K., Kimura, K., Yamashita, R., Itoh, A. and Mizokami, S., 2004. An analysis system for propulsive performance in waves. *Journal of the Kansai Society of Naval Architects, Japan*, *Vol*.241, pp. 1–16. (in Japanese) https://doi.org/10.14856/jksna.2004.67

Kawai, H., Kawaguchi, K. and Fujiki, T., 2020. Half-century-long wave observation in and around Japanese ports through NOWPHAS. *Proceedings of the 30th International Ocean and Polar Engineering Conference*, *ISOPE-2020*, *Vol*.3, pp. 2635–2642. ISBN: 978-1-880653-84-5.

Liang, L., Cheng, Q. and Cai, P., 2022. Design of fin stabilizer controller during ship zig-zag motion. *Ocean Engineering*, *Vol*.252, 111049. https://doi.org/10.1016/j.oceaneng.2022.11049

Lee, S. W., Sasa, K., Aoki, S., Yamamoto, K. and Chen C., 2021. New evaluation of ship mooring with friction effects on mooring rope and cost-benefit estimation to improve port safety. *International Journal of Naval Architecture and Ocean Engineering*, *Vol*.13, pp. 306–320. https://doi.org/10.1016/j.ijnaoe.2021.04.002.

Lee, S. W., Sasa, K., Chen, C., Waskito, K. T. and Cho, I. S., 2022. Novel safety evaluation technique for ships in offshore anchorage under rough seas conditions for optimal ship routing. *Ocean Engineering*, *Vol*.253, 111323. https://doi.org/10.1016/j.oceaneng.2022.111323

Lu, L. F., Sasa, K., Sasaki, W., Terada, D., Kano, T. and Mizojiri, T., 2017. Rough wave simulation and validation using onboard ship motion data in the southern hemisphere to enhance ship weather routing. *Ocean Engineering, Vol*.144, pp. 61–77. https://doi.org/10.1016/j.oceaneng.2017.08.037.

Ministry of Land, Infrastructure, Transport and Tourism, 2011. Safety countermeasure for ferries and Ro/Ro ships. (in Japanese) https://www.mlit.go.jp/report/press/kaiji06_hh_000036.html

Natskår, A., Moan, T. and Alvær, P., 2015. Uncertainty in forecasted environmental conditions for reliability analyses of marine operations. *Ocean Engineering*, *Vol*.108, pp. 636–647. https://doi.org/10.1016/j.oceaneng.2015.08.034.

Newman, J. N., 1979. The theory of ship motions. *Advances in Applied Mechanics*, *Vol*.18, pp. 221–283. http://dx.doi.org/10.1016/S0065-2156(08)70268-0

OCIMF (Oil Companies International Marine Forum), 2018. Mooring equipment guidelines (MEG4), fourth edition, *Witherby Publishing Group Ltd.*

Ota, S., Sakamoto, M., Abe, K. and Nakamura, T., 2000. Study on method for evaluating securing arrangements for Pure Car Carriers: –Numerical model for calculating forces acting on a car and lashing belts. *The Journal of Japan Institute of Navigation*, *Vol.*103, pp. 143–150. https://doi.org/10.9749/jin.103.143

Perez, T. and Goodwin, G.C., 2008. Constrained predictive control of ship fin stabilizers to prevent dynamic stall. *Control Engineering Practice*, *Vol.*16, pp. 482–494. https://doi.org/10.1016/j.conengprac.2006.02.016

Poulios, P., Themelis, N. and Spyrou, K. J., 2008. Dynamics of lashed trailers on board ships under the combined effect of roll and pitch motions. *Maritime Industry, Ocean and Coastal Resources*, pp. 95–106. ISBN: 978-0-415-45523-7

Poulios, P., Themelis, N. and Spyrou, K., 2009. Dynamics of lashed trailers on a ship under roll and pitch excitations. *Journal of Engineering for the Maritime Environment*, *Vol.*223, *Part M*, pp. 1–15. https://doi.org/10.1243/14750902JEME107

Puisa, R., 2018. Optimal stowage on Ro-Ro decks for efficiency and safety. *Journal of Marine Engineering & Technology, Vol.*20, *No.*1, pp. 17–33. https://doi.org/10.1080/20464177.2018.1516942

Saito, K. and Kubo, M., 1996. Basic research on prevention of pull-down cargo by earthquake—slip of an object on oscillating floor, *Journal of Japan Institute of Navigation*, *No.*95, pp. 325–330. (in Japanese) https://doi.org/10.9749/jin.95.325

Saito, K. and Kubo, M., 1997. Basic research on prevention of pull-down of palletized cargo. *Journal of Japan Institute of Navigation*, *No.*96, pp. 275–282. (in Japanese) https://doi.org/10.9749/jin.96.275

Saito, K., Kubo, M. and Kiritoshi, Y., 2002. Slipping motions of pallet-load on vibration. *Journal of Japan Institute of Navigation*, *No.*107, pp. 41–45. (in Japanese) https://doi.org/10.9749/jin.107.41

Sasa, K., Kubo, M., Nagai, T., Yoneyama, H. and Shiraishi, S., 2005. A study on difficulties of entering and departing harbours due to wave induced ship motions. *International Journal of Offshore and Polar Engineering*, *Vol.*15, *No.*2, pp. 117–124. https://doi.org/10.17736/10535381

Sasa K., Terada, D., Shiotani, S. and Kobayashi, E., 2012. A study of numerical simulations of ship motions while underway using a coastal database. *International Journal of Offshore and Polar Engineering*, *Vol.*22, *No.*1, pp. 38–45. ISSN: 1053-5381

Sasa, K., Chen, C., Shiotani, S., Ohsawa, T. and Terada, D., 2014. Numerical analysis of failed forecasts of waves under low pressures from viewpoint of ship operation. *Proceedings of the 33rd International Conference on Ocean, Offshore and Arctic Engineering*, pp. 1–8. https://doi.org/10.1115/OMAE2014-23876

Sasa, K., Faltinsen, O. M., Lu, L. F., Sasaki, W., Prpić-Oršić, J., Kashiwagi, M. and Ikebuchi, T., 2017. Development and validation of speed loss for a blunt-shaped ship in two rough sea voyages in the Southern Hemisphere *Ocean Engineering*, *Vol.*142, pp. 577–596. https://doi.org/10.1016/j.oceaneng.2017.07.029

Sasa, K., Chen, C., Fujimatsu, T., Shoji, R. and Maki, A., 2021. Speed loss analysis and rough wave avoidance algorithms for optimal ship routing simulation of 28,000-DWT bulk carrier. *Ocean Engineering*, *Vol.*228, 108800. https://doi.org/10.1016/j.oceaneng.2021.108800

Sun, X., Wang, S., Wang, Z., Liu, C. and Yin, Y., 2022. A semi-automated approach to stowage planning for Ro-Ro ships. *Ocean Engineering*, *Vol.*247, 110648. https://doi.org/10.1016/j.oceaneng.2022.110648

Takashima, K., Mezaoui, B. and Shoji, R., 2009. On the fuel saving operation for coastal merchant ships using weather routing. *The International Journal on Marine Navigation and Safety of Sea Transportation*, *Vol.*3, *No.*4, pp. 401–406. ISSN 2083-6473

Tolman. H. L., 1989. The numerical model WAVEWATCH: a third-generation model for hindcasting of wind waves on tides in shelf seas. *Faculty of Civil Engineering*, *Delft University of Technology*. ISSN 0169-6548

Tolman. H. L., 2014. User manual and system documentation of WAVEWATCH III Version 4.18. *National Oceanic and Atmospheric Administration/National Weather Service/National Centers for Environmental Prediction (NOAA/NWS/NCEP)*. Technical Note., pp. 282

Turnbull, S. R. and Dawson, D., 1994. The securing of vehicles on roll-on/roll-off ships. *The Royal Institution of Naval Architects 1994*, pp. 37–51.

Turnbull, S. R. and Dawson, D., 1997. The securing of rigid semi-trailers on roll-on/roll-off ships. *International Journal of Mechanical Sciences*, *Vol.*39, *No.*1, pp. 1–14. https://doi.org/10.1016/0020-7403(96)00021-5

Turnbull, S. R. and Dawson, D., 1999. The dynamic behaviour of flexible semi-trailers on board Ro-Ro ship. *International Journal of Mechanical Sciences*, *Vol.*41, pp. 1447–1460. https://doi.org/10.1016/S0020-7403(98)00106-4

Turnbull, S. R., 2000. Roll-on/roll-off semi-trailer models: a comparison of results. *Journal of Marine Science and Technology*, *Vol.*5, pp. 101–106. https://doi.org/10.1007/s007730070006

Waskito, K. T., Sasa, K., Chen, C., Kitagawa, Y. and Lee, S. W., 2022. Comparative study of realistic ship motion simulation for optimal ship routing of a bulk carrier in rough seas. *Ocean Engineering, Vol.*260, 111731. https://doi.org/10.1016/j.oceaneng.2022.111731.

Yakabe, F., Ota, S. and Tamura, K. 2013. Study on methods to evaluate effectiveness of securing arrangements for Semi-Trailers on Ro-Ro ferries. *The Journal of Japan Institute of Navigation*, *Vol.*128, pp. 89–100. (in Japanese) https://doi.org/10.9749/jin.128.89

Zhang, D., Tang, Y., Clarke, D. B., Peng, Q. and Dong, C., 2019. An innovative method for calculating diagonal lashing force of cargo on railway wagons in a curve alignment. *International Journal of Vehicle Mechanics and Mobility*, *Vol.*59, *No.*3, pp. 352–374. https://doi.org/10.1080/00423114.2019.1686160

Appendix. Nomenclature

List of abbreviations

AIS	Automatic identification system
ECMWF	European Centre for Medium-Ranged Weather Forecast
EUT	Enhanced unified theory
GPS	Global positioning system
LNGC	Liquefied natural gas carriers
NOWPHAS	Nationwide Ocean Wave information network for Ports and HAbourS
NCEP-FNL	National Centers for Environmental Prediction Final
VLCC	Very large crude carriers

WW3	WaveWATCH III

List of symbols

A_L, A_R	Distance between the lashing point on the deck and the spine on the left and right sides
B_L, B_R	Width of the trailer at lashing wire on left and right sides
B_S	Half-widths of the trailer body at the suspension
C_{Li}, C_{Ri}	Length of each lashing wire in longitudinal direction (*x*-axis) on left and right sides
C_{Ry}, C_{Rz}	Centrifugal force owing to ship roll motion along the *y*- and *z*-axes
C_{Px}, C_{Pz}	Centrifugal forces owing to ship pitch motion along the *x*- and *z*-axes
D	Directional function
E_W	Wave directional spectrum
E_R	Directional spectrum in ship roll motion
E_P	Directional spectrum in ship pitch motion
f	Wave frequency
F_{Line}	Load applied to the lashing wire
F_{Li}, F_{Ri}	Load applied to the lashing wire on the left and right sides.
F_{LXi}, F_{RXi}	Horizontal force acting on each lashing wire on the left and right sides
F_{LYi}, F_{RYi}	Lateral force acting on each lashing wire on the left and right sides
F_{LZi}, F_{RZi}	Vertical force acting on each lashing wire on the left and right sides
F_{SL}	Load applied to the suspension on the left side
F_{SR}	Load applied to the suspension on the right side
F_S	Total force on the suspension
I_{Pitch}	Inertial moment of pitch motion of trailer
I_{Roll}	Inertial moment of roll motion of trailer
K_S	Suspension spring stiffness coefficient
K_{Line}	Spring constant for lashing wire
L_{Li}, L_{Ri}	Length of each lashing wire on the left and right sides
L_0	Initial length of lashing wire
m	Mass of trailer
P	Frequency response function in pitch motion of ship
$P_{1/3}$	Significant amplitude in pitch motion of ship
P_{SHIP}	Pitch motion of ship in time series
P_T	Pitch motion of trailer
r_1	Distance from the center of gravity of ship to the center of the trailer in the *y*-*z* plane
r_2	Distance from the center of gravity of ship to the center of the trailer in the *x*-*z* plane
R	Frequency response function in roll motion of ship
$R_{1/3}$	Significant amplitude in roll motion of ship
R_{SHIP}	Roll motion of ship in time series

R_T	Roll motion of trailer
R_{Rx}, R_{Ry}, R_{Rz}	Total force acting on the trailer due to the roll motion along the *x, y*, and *z* axes
R_{Px}, R_{Py}, R_{Pz}	Total force acting on the trailer owing to pitch motion along the *x, y*, and *z* axes
S_{Li}, S_{Ri}	Length of each lashing wire in the transverse direction (*y*-axis) on the left and right sides.
S_W	Wave frequency spectrum
T_{Li}, T_{Ri}	Length of each lashing wire in the vertical direction (*z*-axis) on the left and right sides.
T_{Ry}, T_{Rz}	Tangential force due to ship roll motion along the *y*- and *z*-axes
T_{Px}, T_{Pz}	Tangential forces owing to ship pitch motion along the *x*- and *z*-axes
X_L, X_R	Horizontal distance between lashing point and center of gravity on the left and right sides
X_S	Horizontal distance of suspension from its longitudinal center of gravity
x, y, z	Motions of the trailer along the *x, y,* and *z* directions
Z_G	Vertical distance between the mass and spine
Z_H	Height of the suspension
Z_L, Z_R	Vertical distance between the spar and spine on the left and right sides
Z_S	Vertical distance of mass from the deck
Z_{SS}	Vertical distance between the top of suspension and the spine
β	Angle between the center of gravity of the ship and the center of the trailer in the *y-z* plane
δ	Angle between the center of gravity of the ship and the center of the trailer in the *x-z* plane
ε	Phase of incident wave
ε_R	Phase in roll motion of ship
ε_P	Phase in pitch motion of ship
θ	Incident wave direction
θ_0	Main wave direction
λ_S	Suspension damping coefficient
μ_S	Friction coefficient between tire and deck